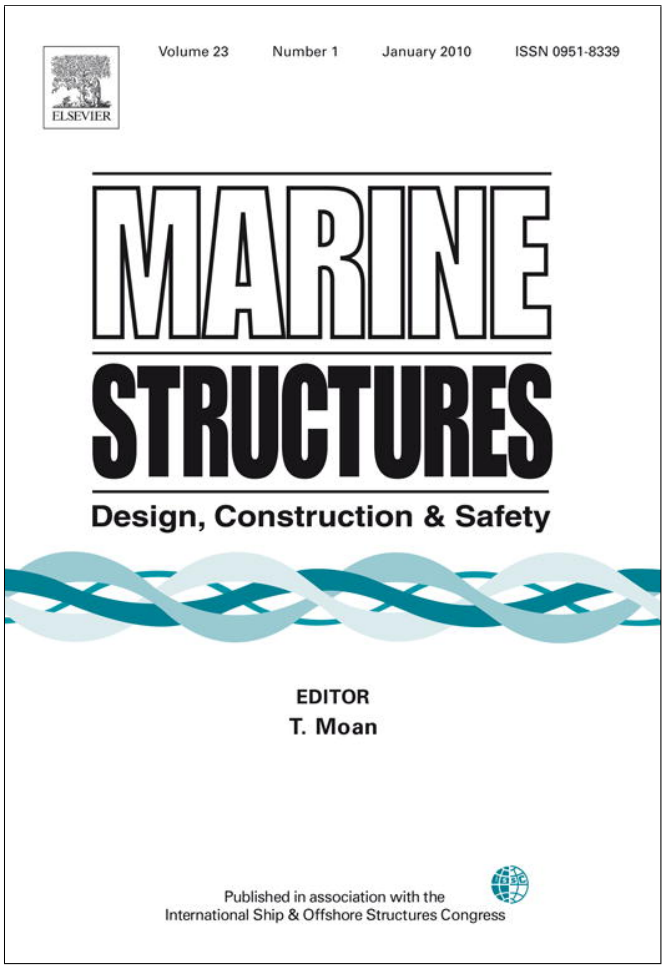

Marine Structures 23 (2010) 39–66

Contents lists available at ScienceDirect

Marine Structures

journal homepage: www.elsevier.com/locate/marstruc

# Post-buckling behaviour and strength of multi-stiffened aluminium panels under combined axial compression and lateral pressure

Mohammad Reza Khedmati [a,*], Abbas Bayatfar [b], Philippe Rigo [c]

[a] Faculty of Marine Technology, Amirkabir University of Technology, Hafez Ave., No. 424, Tehran 15914, Iran
[b] Azad University, Aligudarz, Iran
[c] University of Liège, ANAST, Chemin des Chevreuils 1 (B52/3), 4000 Liège, Belgium

ARTICLE INFO

*Article history:*
Received 4 March 2009
Received in revised form
13 September 2009
Accepted 19 October 2009

*Keywords:*
Buckling load
Ultimate strength
Post-buckling behaviour
Multi-stiffened aluminium panels
Axial compression
Lateral pressure
Heat-affected zone
Finite Element Method (FEM)

ABSTRACT

This paper presents the results of complementary numerical study done in the continuation of the activities carried out by the Committee III.1 "Ultimate Strength" of ISSC'2003 (Ref. [28] ).The main focus of the paper concerns the post-buckling behaviour and strength characteristics of the aluminium multi-stiffened panels under combined axial compression and lateral pressure.

The finite element model proposed by the Committee III.1 "Ultimate Strength" of ISSC'2003 is used in the present investigation. Material is aluminium alloy AA6082-T6 and the multi-stiffened panel is a triple-span structure. Stiffeners are of either extruded or non-extruded angle-bar profiles. An initial deflection is imposed on the model in a procedure similar to that applied by the Committee III.1. General purpose finite element code ANSYS is used for non-linear elastic–plastic analyses.

Main objectives are to study the influence of initial deflections and also HAZ on the post-buckling behaviour and collapse characteristics of aluminium stiffened panels under combined axial compression and lateral pressure. Different values of lateral pressure are exerted on the model in a systematic manner to simulate various levels of lateral pressure loading on multi-stiffened aluminium panels used in the construction of high-speed crafts.



* Corresponding author. Tel.: +98 21 64543113; fax: +98 21 66412495.
*E-mail address:* khedmati@aut.ac.ir (M.R. Khedmati).

0951-8339/$ – see front matter © 2009 Elsevier Ltd. All rights reserved.
doi:10.1016/j.marstruc.2009.10.003

**Notation**

| | |
|---|---|
| $L$ | overall length of plate |
| $b$ | overall breadth of plate |
| $t$ | plate thickness |
| $t_w$ | Thickness of longitudinal stiffener web |
| $h_w$ | height of longitudinal stiffener web |
| $t_f$ | thickness of longitudinal stiffener flange |
| $b_f$ | breadth of longitudinal stiffener flange |
| $t_{wt}$ | thickness of transverse frame web |
| $h_{wt}$ | height of transverse frame web |
| $t_{ft}$ | thickness of transverse frame flange |
| $b_{ft}$ | breadth of transverse frame flange |
| $\nu$ | Poisson's ratio |
| $E$ | Young's modulus |
| $\sigma_Y$ | yield stress |
| $\sigma_{iY}$ | initial yielding stress |
| $\sigma$ | average stress |
| $\varepsilon$ | average strain |
| $\theta_x$ | rotation about $x$-axis |
| $\theta_y$ | rotation about $y$-axis |
| $\theta_z$ | rotation about z-axis |
| $U$ | displacement along $x$-axis |
| $V$ | displacement along $y$-axis |
| $W$ | displacement along $z$-axis |
| {R} | load vector |
| [K] | conventional stiffness matrix |
| {D} | vector of nodal displacements and rotations |

## 1. Introduction

Stiffened plates are used as main supporting members in many civil as well as marine structural applications. They typically consist of a plate with equally spaced stiffeners welded on one side, often with intermediate transverse stiffeners or bulkheads. The most common stiffener cross-sections are bulb, flat bar or T- and L-sections. Such structural arrangements are common for both steel and aluminium structures.

Due to HAZ effects, aluminium alloys are more sensitive to welding in comparison with steel, and multi-stiffened plate panels build with direct welding of stiffeners to the plate exhibit less strength under in-plane loads.

However, developments in extrusion technology have opened up opportunities for new designs in aluminium. Here, panels fabricated from extruded aluminium elements welded by improved welding methods (such as STIR welding) have led to significant improvements in geometric tolerances, increased structural efficiency and reduced costs. These extruded elements may contain one or more stiffeners in their structure.

Aluminium panels have been used in a variety of marine structures, with applications such as hull and decks in high-speed boats and catamarans and superstructures for ships. Other applications are box-girder bridges, and walls and floors in offshore modules and containers. These panels are primarily required to resist axial compressive forces, even though transverse loads and in-plane shear forces may in general interact.

Compared to steel, relatively little experience has been accumulated for large aluminium structures, and the existing design recommendations for aluminium panels are to a large extent based on experience from steel structures. This means that the effect of improved tolerances and the possibility of more efficient stiffener designs are not adequately taken into account in the design recommendations. On the other hand, the alloy-dependent material properties and the possibly detrimental effect of welding may not be adequately represented in the codes.

The ultimate strength of stiffened steel plate panels has been the subject of many investigations, both experimentally [1–11] and numerically [12–19], with the most significant contributions in the field of ship structures and bridges. The literature on stiffened aluminium panels is more limited. Clarke [20] reports on buckling tests on an aluminium AA5083 plate with welded T-bar and flat bar stiffeners. His experimental programme comprised eight compression tests on panels with different plate and stiffener sizes, with buckling over two spans as the failure mode. The ultimate strength of stiffened aluminium AA6082-T6 plates under the axial compression was investigated by Aalberg et al. [21,22] using numerical and experimental methods. Kristensen and Moan [23] demonstrated numerically the effect of HAZ and residual stresses on the ultimate strength of rectangular aluminium plates (AA5083 and AA6082) under the bi-axial loading of plates. Some initial experimental and numerical simulations on torsional buckling of flatbars in aluminium panels have been also presented by Zha and Moan [24–26]. Hopperstad et al. [27] carried out a study with the objective of assessing the reliability of non-linear finite element analyses in predictions on ultimate strength of aluminium plates subjected to in-plane compression. Rigo et al. [28] made a numerical investigation to present reliable finite element models to study the behaviour of axially compressed stiffened aluminium panels (including extruded profiles). Also Paik and Duran [29] made a numerical study on some welded aluminium panels under in-plane compression and derived an empirical equation to estimate the ultimate strength of them.

Most of the aforementioned studies are just focused on the investigation of either buckling or ultimate strength characteristics of the stiffened aluminium plate panels. Also only the case of in-plane compression has been considered as applied loading condition of the stiffened plate panels. Post-buckling behaviour and strength of such stiffened panels under combined in-plane compression and lateral pressure have not been addressed yet to our knowledge.

This paper presents the results of a numerical study following the activities carried out by the Committee III.1 ‘‘Ultimate Strength’’ of ISSC’2003. The main focus of the paper lies on the investigation of the post-buckling behaviour and strength characteristics of the aluminium multi-stiffened panels under combined axial compression and lateral pressure.

The finite element model proposed by the ISSC’2003Committee III.1 is applied in the present investigation. Material is aluminium alloy AA6082-T6 and the model is multi-stiffened. Stiffeners are of either extruded or non-extruded angle-bar profiles. An initial deflection is imposed on the model in a procedure similar to that applied by the Committee III.1. General purpose finite element code ANSYS is used for non-linear elastic–plastic analyses.

Main objectives are to study the influence of initial deflections and also HAZ on the post-buckling behaviour and collapse characteristics of aluminium stiffened panels under combined axial compression and lateral pressure. Lateral pressure on the multi-stiffened aluminium plate may have different levels. When the high-speed craft is floating on still water, hydrostatic lateral pressure acts on the multi-stiffened aluminium plates. Besides, when the craft is moving amongst waves, hydrodynamic or wave-induced lateral pressure acts on the structure under consideration. The analyses in this study have been made for different levels of lateral pressure which may correspond to either hydrostatic or hydrodynamic levels of lateral load.

## 2. Models for analysis

### 2.1. Structural arrangements and geometrical characteristics

A three-span plate with L-shaped stiffeners fabricated from aluminium profiles in alloy AA6082 temper T6, joined by welding, was considered for the finite element analyses by Rigo et al. [28].

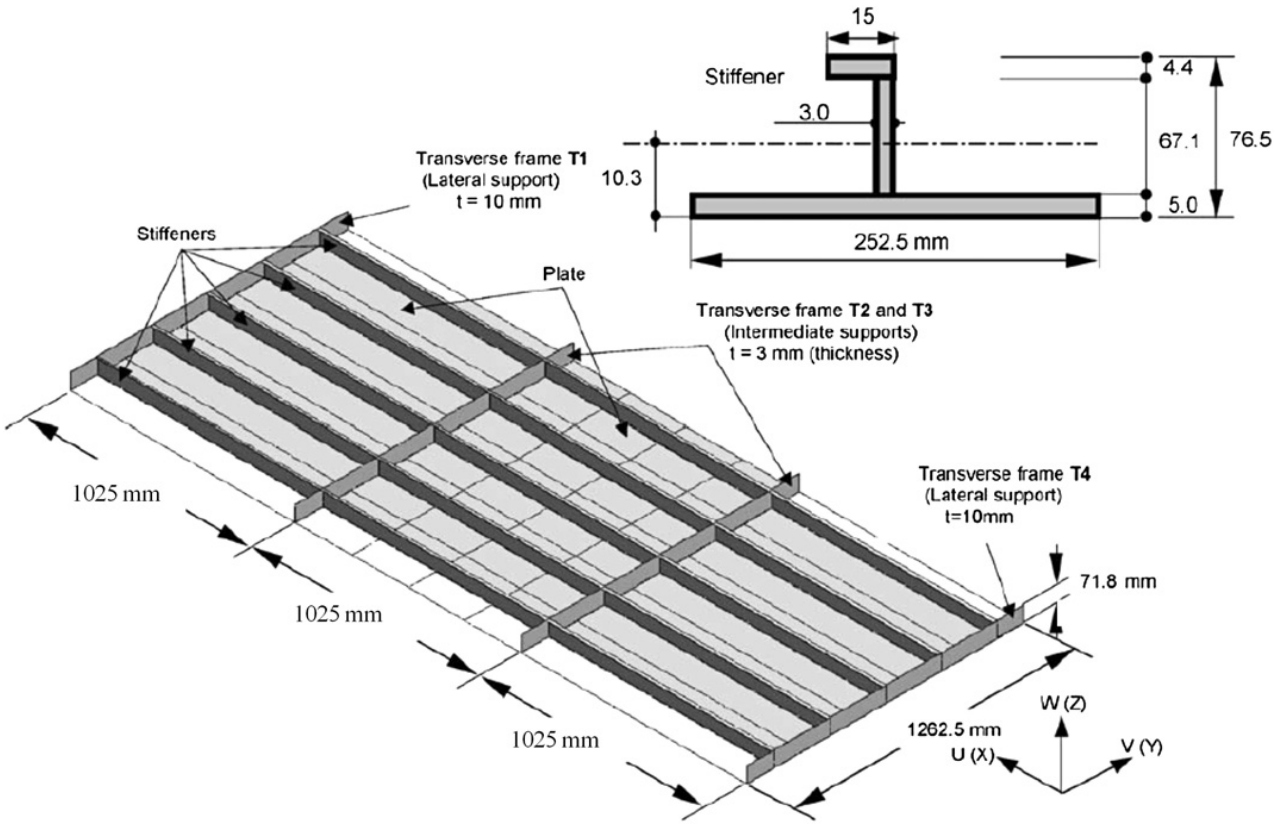


**Fig. 1.** The three-span model used in the benchmark study of Rigo et al. [28].

The same model was considered in the present investigation. The dimensions of the initial model are shown in Fig. 1 with the XYZ coordinate system and the U–V–W corresponding displacements.

Rigo et al. performed a detailed benchmark study on the ultimate strength of stiffened aluminium plates under in-plane compression [28]. The target of their benchmark study was to present reliable finite element models to study the behaviour of axially compressed stiffened aluminium plates (including extruded profiles). Main objectives were to compare codes/models and to perform quantitative sensitivity analysis of the ultimate strength of a welded aluminium plate on various parameters (typically the heat-affected zone).

### 2.2. Finite element code and adopted elements

The commercial finite element code ANSYS [30] is used for all analyses. Among the elements inside the library of ANSYS, the SHELL43 elements were selected in order to discretise the stiffened plate models. SHELL43 is well suited to model linear, warped, moderately-thick shell structures. The element has six degrees of freedom at each node: translations in the nodal $x$, $y$, and $z$ directions and rotations about the nodal $x$, $y$, and $z$ axes. The deformation shapes are linear in both in-plane directions. For the out-of-plane motion, it uses a mixed interpolation of tensorial components. The element has plasticity, creep, stress stiffening, large deflection, and large strain capabilities [30].

### 2.3. Mechanical properties of material

The material used in the study is aluminium alloy 6082-T6 and its mechanical properties are given in Table 1. The average stress–average strain curve of this alloy is shown in Fig. 2.

**Table 1**
Summary of material properties.

| $E$ | $\upsilon$ | $\sigma_Y$ |
|---|---|---|
| MPa | – | MPa |
| 70,475 | 0.3 | 260 |

### 2.4. Boundary and loading conditions

In the present FE computations, as proposed by Rigo et al. [28], the boundary conditions of the stiffened plates are assumed simply supported along the two longitudinal edges (unloaded), which are kept straight (constrained edges).

The loaded edges were restrained from rotation and an axial displacement was prescribed ($W = V = 0$ and restrained rotation $\theta_y = 0$, with $U = 0$ on one side and $U = U^*$ on the other side). At these two loaded edges, the stiffener cross-section remains plane as the stiffened plate was supported by stiff transverse frames. The two end frames (T1 and T4) were assumed perfectly rigid (Fig. 1) and were modelled by thick transverse plates. Their dimensions were $1262.5 \times 71.8$mm2 and thickness 10 mm.

At the intermediate support locations, transverse plates were also provided, T2 and T3 with thickness of 3 mm (Fig. 1). Then, the five longitudinal stiffeners were supported by the two intermediate and the two end plates (frames); the sideways deformation of the stiffeners not being allowed. This means that V is restrained at 4 points ($V = 0$ at $Y = 0$) in the main plate, along the symmetry axis (Fig. 3). Also, unloaded longitudinal edges remain straight ($V =$ constant along these 2 edges). In order to simulate stiff transverse frames, the displacements (W) along Z of these four transverse plates were not allowed. $W = 0$ was assumed for all the nodes at the intersection between the main plate and the four transverse support plates (Fig. 3).

In case of pure in-plane compression, uniform in-plane displacement is imposed on one of the loaded edges while the other loaded edge is restrained against in-plane movement. When lateral pressure exists in addition to in-plane compression, first the lateral pressure is applied incrementally up to the relevant value and then uniform in-plane displacement is exerted on the model in an incremental way.

### 2.5. Initial imperfections

To consider the initial deflection of the model, the procedure described in the study of Rigo et al. [28] was adopted. Uniform lateral pressure was applied first on the stiffened plate model and a linear

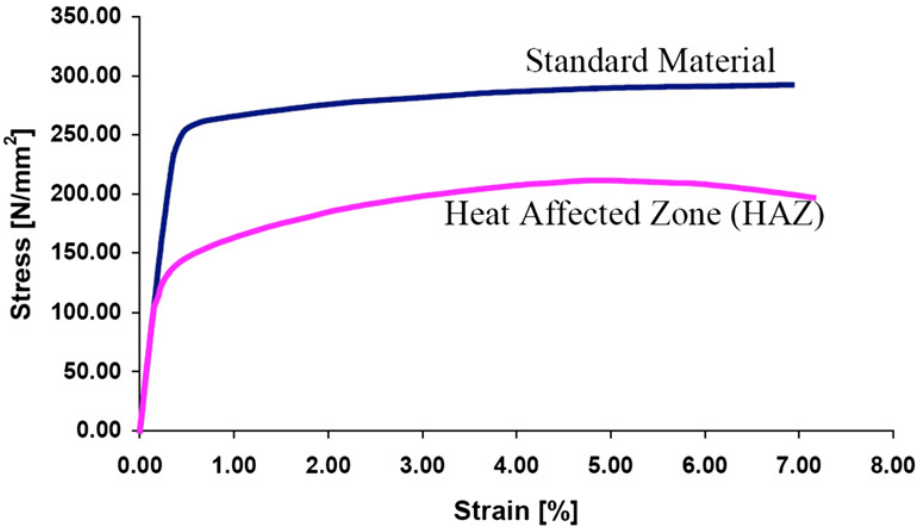


**Fig. 2.** Average stress–average strain curve of the aluminium material in standard state and also in HAZ.

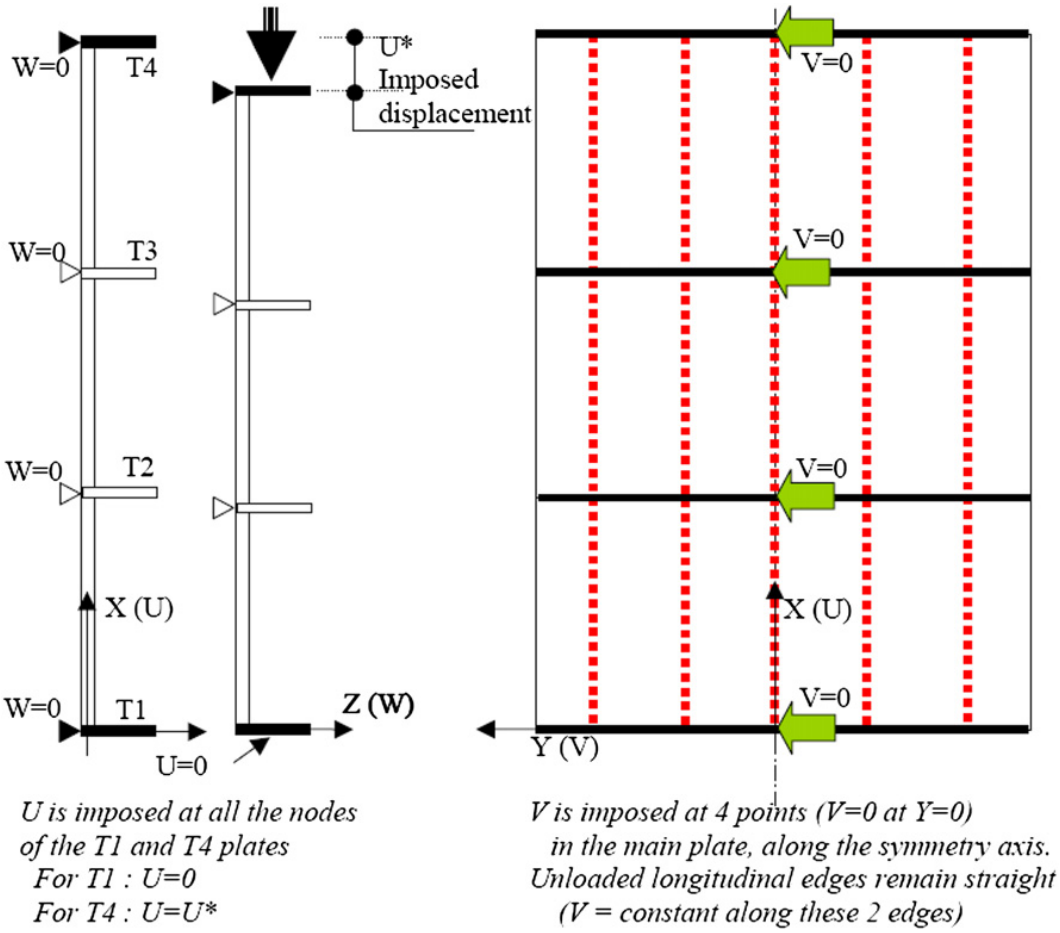


**Fig. 3.** Boundary conditions of the Rigo et al. model [28].

elastic finite element analysis was carried out. This analysis was repeated in a trial and error sequence of calculations so that the magnitude of maximum deflection of plate reached 2 mm (Fig. 4). The FE model with resulting deformation mode is adopted as the model for performing non-linear analyses under the action of longitudinal in-plane compression.

### 2.6. Analysed cases with respect to welding-induced HAZ

Five different cases as shown in Fig. 5 are considered for the analysis purposes. They are described with some details below:

- The case without considering Heat-Affected Zone (HAZ), called as "model without HAZ". This case is analysed as reference case.
- The case with welds A in which five longitudinal welds along the junction lines between the plate and five stiffeners exist, called as "model A".
- The case with welds B in which four longitudinal welds at the intersection between the five extruded elements exist, called as "model B".
- The case in which in addition to the welds A, one line of transversal weld C also exist, called as "model A + C".
- The case in which in addition to the welds B, one line of transversal weld C also exist, called as "model B + C".

HAZ width = 2 × 25 mm in plating and 25 mm in stiffener web plate measured from midplane of plate, Fig 6.

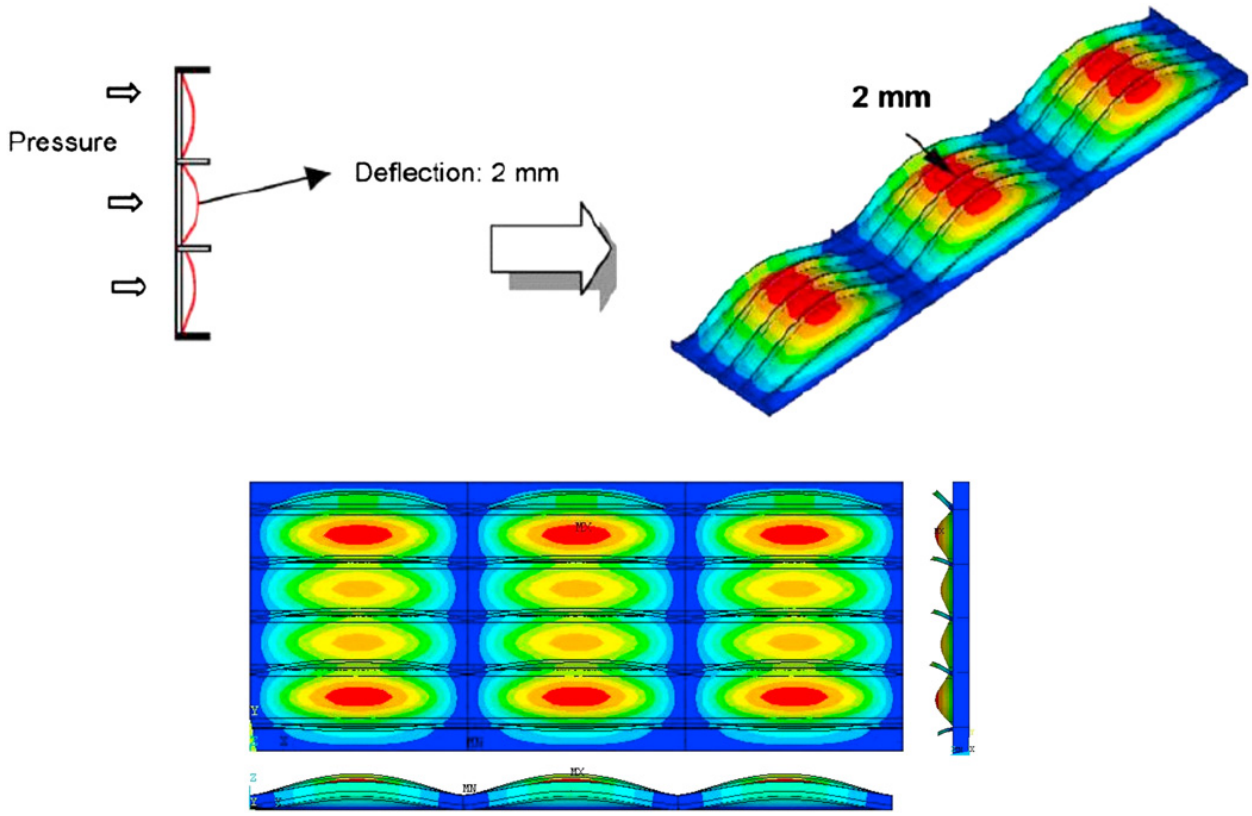


**Fig. 4.** Procedure to define the initial deflection (top) [28] and a snapshot of the initial deflection mode (down).

### 2.7. Tracing the average stress–average strain relationship

Calculation of the ultimate strength or limit load of a structural model is inherently a non-linear problem. In general, the non-linear behaviour admits a wide variety of phenomena, possibly interacting with one another and in most cases each difficult to calculate. In structural mechanics, types of nonlinearity include mainly the following

- Material nonlinearity, in which material properties are functions of the state of stress or strain. Examples are yielding or non-linear elasticity.
- Geometric nonlinearity, in which deformation is large enough that equilibrium equations must be written with respect to the deformed structural geometry. Also, loads may change direction as they increase, as when pressure inflates a membrane.

Problems in these categories are nonlinear because stiffness and perhaps loads as well, become functions of displacement or deformation. Thus in structural equations $[K]\{D\} = \{R\}$, coefficient matrix $[K]$ and perhaps load vector $\{R\}$ become functions of $\{D\}$. We cannot immediately solve for $\{D\}$ because information needed to construct $[k]$ and $\{R\}$ is not known in advance. An iterative process is required to obtain $\{D\}$ and it's associated $[K]$ and $\{R\}$ such that the product $[K]\{D\}$ is in equilibrium with $\{R\}$. When equations $[K]\{D\}=\{R\}$ are nonlinear the principle of superposition does not apply. That is, we cannot scale results in proportion to load or superpose results of different load cases.

There are some equation-solving techniques applicable to the above-mentioned non-linear equations. Reference may be made to Cook et al. [31] and Paik et al. [32]. Among such techniques are the following

- Newton–Raphson method
- Modified Newton–Raphson method
- Arc-Length method

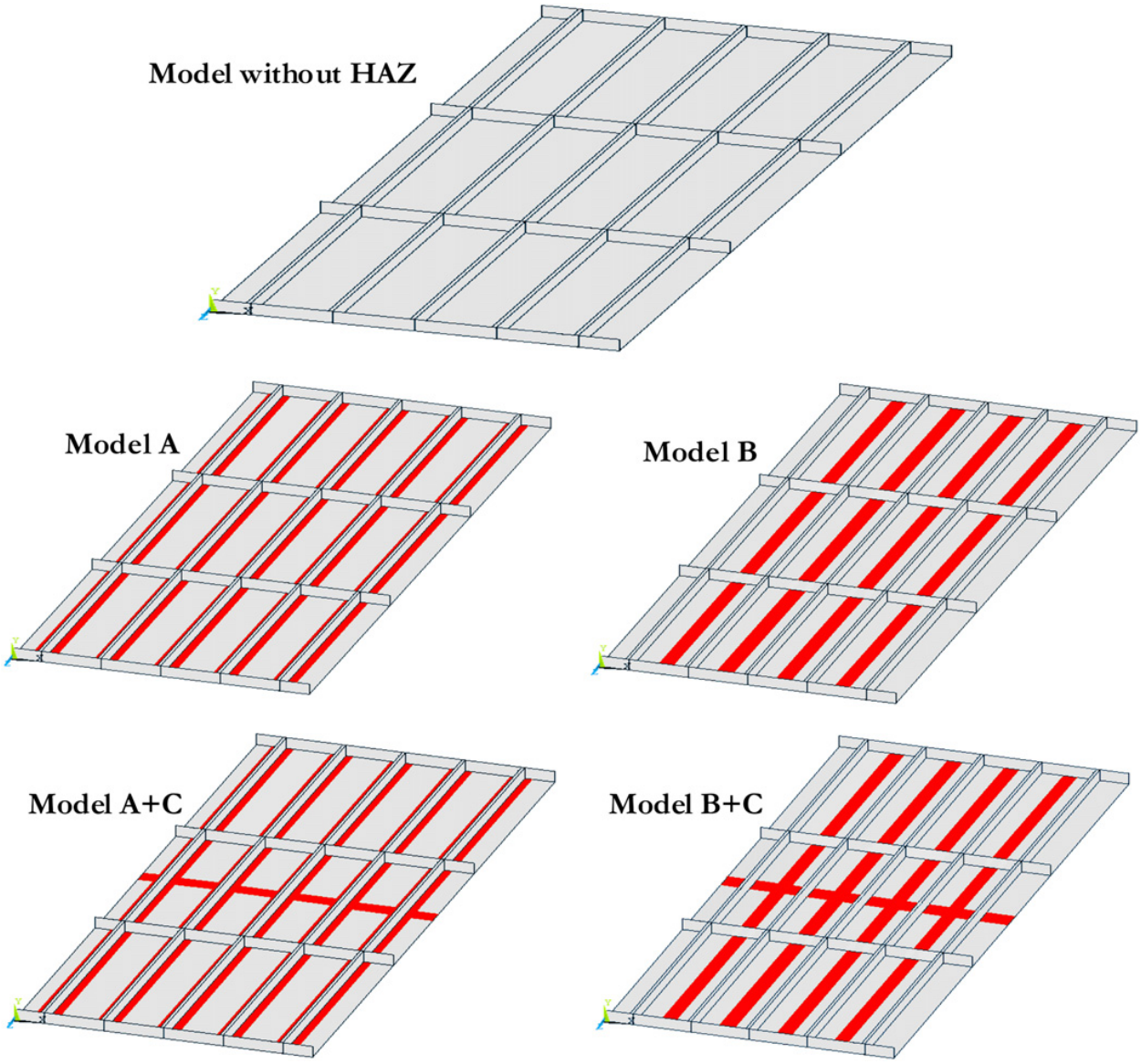


**Fig. 5.** Analysed cases with respect to welding-induced HAZ.

The non-linear responses of the present models are obtained using Newton–Raphson method. Both material and geometric nonlinearities are considered in the analyses.

## 3. Results and discussions

### *3.1. Post-buckling strength and behaviour under pure in-plane axial compression*

Non-linear elastic–plastic finite element analysis is performed for all of the cases shown in Fig. 5 (described in Subsection. 2.6), under pure in-plane compression. Average stress–average strain relationships for all models in addition to their deflection modes and spreads of yielding at different steps of loading are obtained from such analyses and shown with details in Figs. 7–11. As can be seen from Figs. 7–11(a), the trend and accuracy of the average stress–average strain curves obtained based on the present analyses are in good agreement with those obtained by other researchers as quoted in ref. [28]. To avoid any confusing in reading Figs. 7–11(a), it should be written that "Rigo et al.", "Lehmann et al." and "Yao et al." in the legend of these figures stand for "Rigo and Sarghiuta", "Lehmann and Catalin" and "Yao and Higashiyama" in the ref. [28].

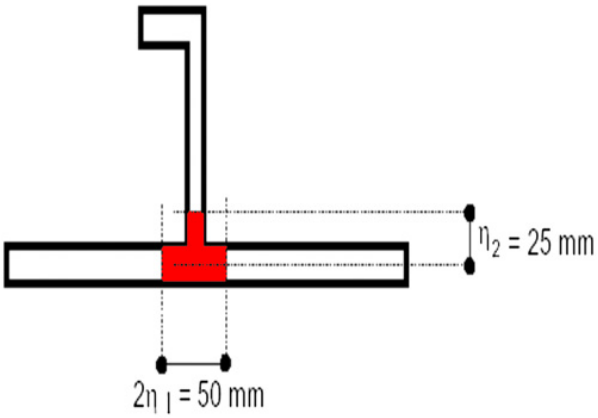


**Fig. 6.** Standard HAZ width ($2\eta_1$ in plate = 50 mm, $\eta_2$ in stiffener web = 25 mm).

Table 2 represents a summary of all results regarding the ultimate strength of all models in comparison with the results of different researchers as reported in ref. [28]. Also a comparison of initial yielding stress values for different models under pure in-plane compression based on the results of present work is shown in Fig. 12. Fig. 13 shows a comparison of the values of the ultimate strength of all models under pure in-plane compression based on the results of different researchers. The trends of average stress–average strain relationships for all models are compared with each other in Fig. 14. In what follows, post-buckling behaviour and strength characteristics of all models are described in more details.

*3.1.1. Model without HAZ*

This model is analysed as a reference case for establishing a comparison basis for other practical cases. The model buckles at a stress level of $0.46\sigma_Y$. Both plate and stiffeners are locally buckled in all spans simultaneously, Fig. 7(b). Considering the difference in boundary conditions around local plate panels in the model, it can be well understood that the deflection modes of these plate panels would differ with each other. Local plate panels in the model exhibit four half-waves in their buckling mode. Such a buckling mode for all panels is gradually completed with growing of the applied force. Along with the buckling of plate panels, buckling of longitudinal stiffeners with three half-waves in each span and also that of transverse frames almost with one half-wave in each bay is observed.

Initial yielding of the model takes place when the applied stress reaches $0.54\sigma_Y$. The onset of yield is appeared in the crest of lower buckling half-waves of the local plate panels and also to some extent in the junction points of longitudinal stiffeners and transverse frames. The model reaches its ultimate strength at the applied stress level of $0.64\sigma_Y$. Fig. 7(c) shows how the local plate panels as well as the longitudinal stiffeners and transverse frames deflect in a simply-supported manner at the maximum load carrying capacity level of the model. Yielding is distributed evenly in the model. At the final step of calculation, Fig. 7(d), the plasticity is accumulated in some parts while unloading takes place in some other regions.

*3.1.2. Model A*

Model A consists of softened heat-affected zones along the junction lines of longitudinal stiffeners and plate. Buckling occurs when the applied stress level reaches $0.45\sigma_Y$, Fig. 8(a). Local buckling of plate panels as well as buckling of longitudinal stiffeners and transverse frames are observed in the buckling mode of the model, Fig. 8(b). Magnitude of torsional deformations in both longitudinal stiffeners and transverse frames in the central part of the model is much more than that in the surroundings of the model. Existence of softened heat-affected zones along stiffeners pronounces the simply-supported boundary conditions for the plate panels.

Yielding in the model members start at the stress level of $0.48\sigma_Y$. When the applied stress reaches $0.56\sigma_Y$, the state of the ultimate strength of the model is obtained. Less regularity in the deflection mode of all members consisting of plate panels, longitudinal stiffeners and transverse frames at the

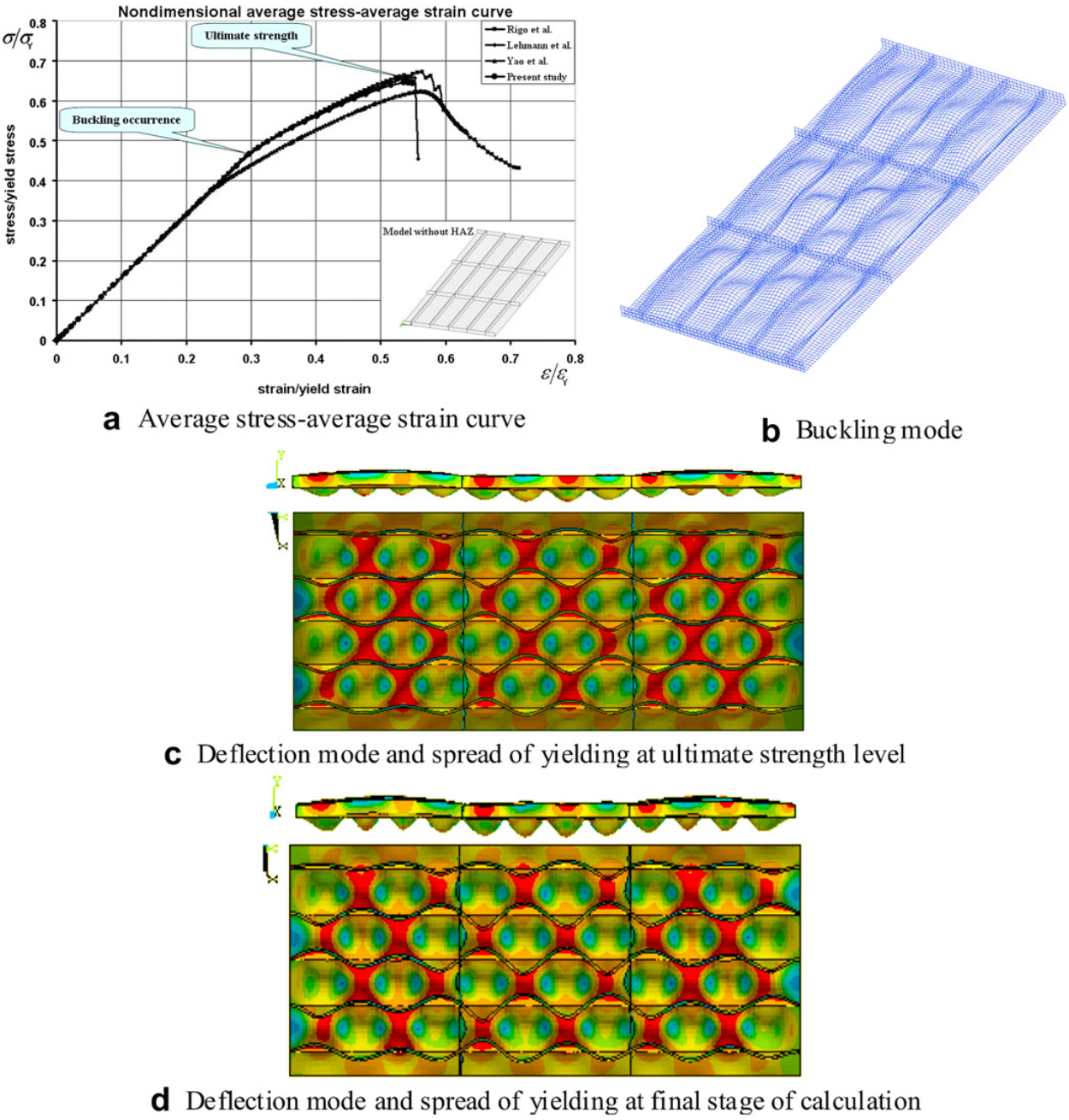


**Fig. 7.** Analysis results for model without HAZ under pure in-plane compression.

ultimate strength level is observed in comparison with the model without HAZ, Fig. 8(c). At the final step of calculation, Fig. 8(d), simply supported overall deflection of the whole model between transverse frames is observed, while unloading takes place in the stiffening members.

### 3.1.3. Model B

In model B, extruded longitudinal stiffeners are used. Therefore, there are four weld lines in the model. This causes the model buckle in a load stress equal to $0.45\sigma_Y$, Fig. 9(a). Buckling mode of the model consist of irregular half-waves in both plate and stiffening members, Fig. 9(b).

With further increase in the magnitude of in-plane compressive load, the deflection mode of the model shows interesting characteristics. Yielding of the model starts at $0.48\sigma_Y$, while its maximum load carrying capacity reaches at the stress level of $0.61\sigma_Y$. At the ultimate strength state, Fig. 9(c), four buckling half-wave in the surrounding panels of model are observed while in the central plate panels

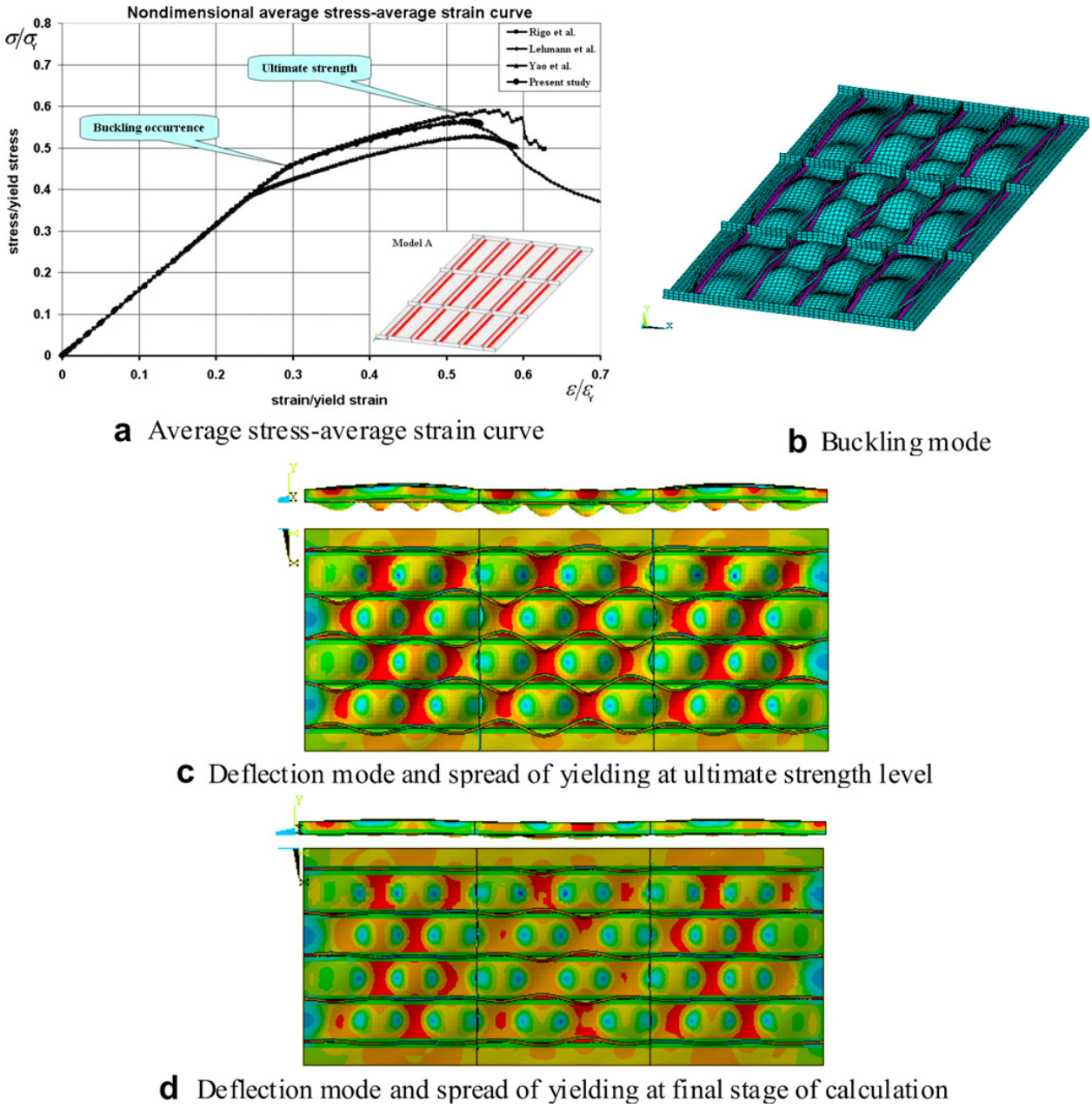


**Fig. 8.** Analysis results for model A under pure in-plane compression.

the number of buckling half-waves is equal to five. Existence of the heat-affected zone just in the middle of central panels leads to the reduction of their breadth. Thus, the effective aspect ratio of these panels reaches to five and finally five buckling half-waves are produced in them. At the final stage of calculation, Fig. 9(d), an interesting overall deflection in the model is seen. This consists of semi-clamped overall deflection of the model at the T1 and T4 locations, decrease in the magnitude of deflections of plate and its stiffening members between T2 and T3 frames and also local tripping of longitudinal stiffeners in neighborhood of T2 and T3 frames in the first and third spans (as shown in Fig. 9(d) by arrows). Due to such a type of collapse mode, local plastic hinges are created in the location of arrows in Fig. 9(d).

### 3.1.4. *Model A + C*

Buckling of this model occurs at the stress level of $0.45\sigma_Y$ as shown in the average stress–average strain relationship, Fig. 10(a). Plate panels as well as longitudinal stiffeners exhibit local deformations which differ somewhat with each other depending on the location in the model, Fig. 10(b).

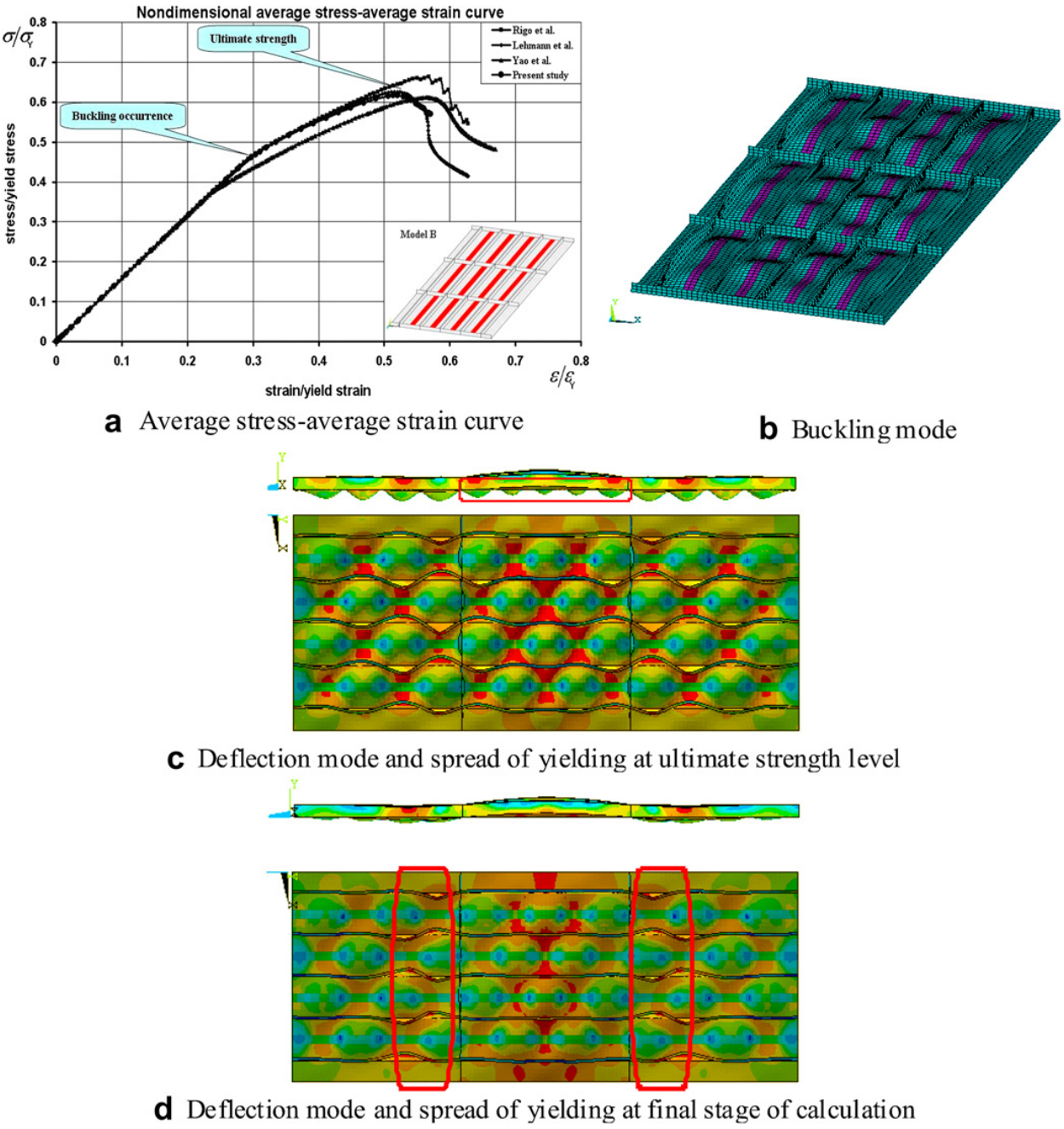


**Fig. 9.** Analysis results for model B under pure in-plane compression.

Yielding occurs at the stress level of $0.48\sigma_Y$. The extent of plasticity is grown in the first and third spans at the ultimate strength level of $0.52\sigma_Y$, Fig. 10(c). At the final step of calculation, Fig. 10(d), severe tripping of longitudinal stiffeners outside the middle span as well as accumulation of local plastic deformations in the middle span are observed while most of the model undergoes unloading. This is a new collapse behaviour in which plastic hinges are created in the stiffeners outside of middle span and in plate inside the middle span. As a result, it can be said that according to the mechanism of three hinge lines, the collapse of the whole model is experienced.

### *3.1.5. Model B + C*

More or less the same as explained for the model A + C is observed for the model B + C under pure in-plane compression. Buckling occurs at the stress level of $0.45\sigma_Y$, Fig. 11(a). Buckling mode of the model consist of magnified deflections of the plate and stiffening members especially in the middle span while the amplitude of such deflections outside the middle span takes a kind of uniformity, Fig. 11(b).

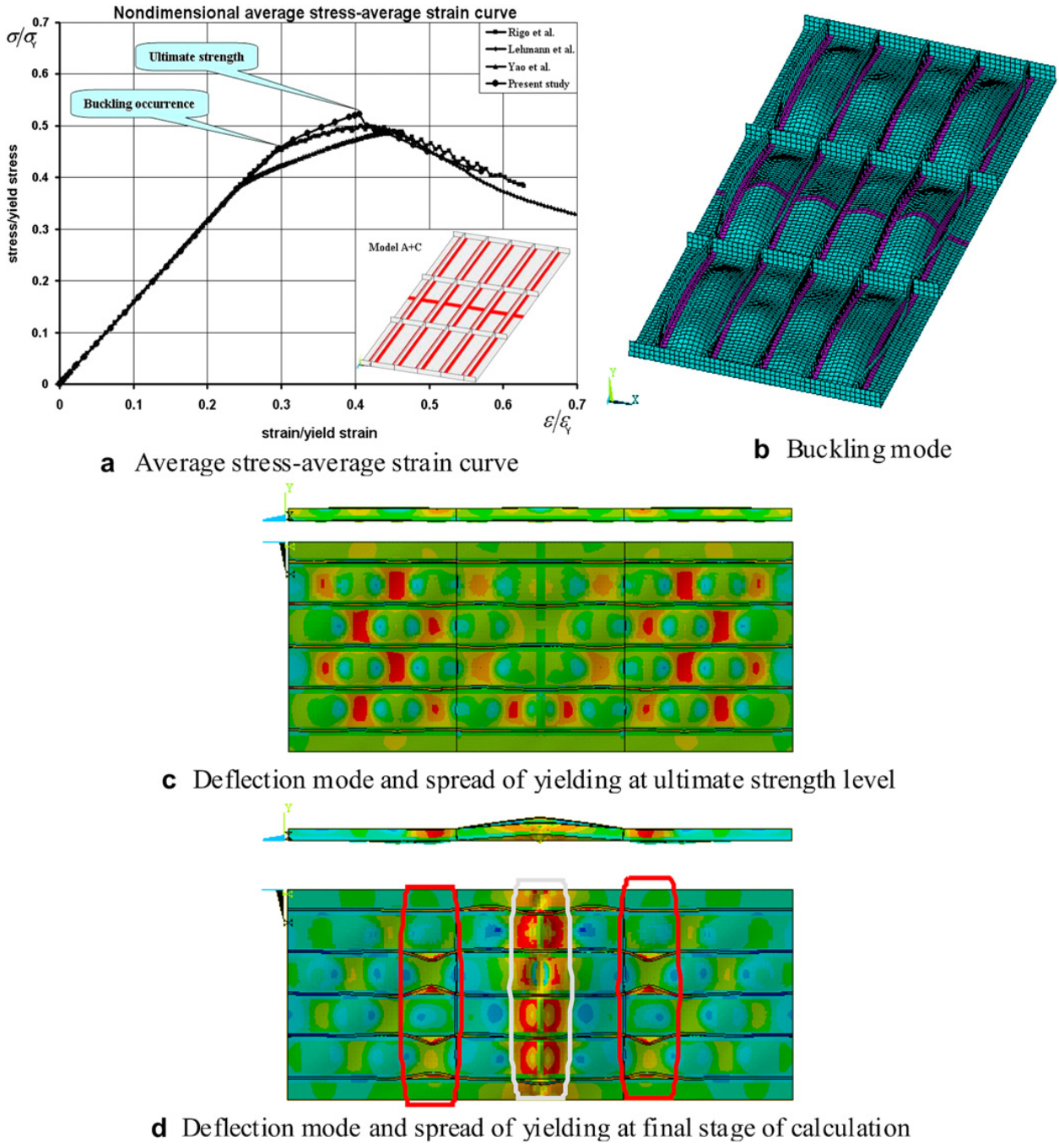


**Fig. 10.** Analysis results for model A + C under pure in-plane compression.

Yielding of the model is seen at the stress level of $0.47\sigma_Y$. With further increase in the applied load, the model reaches its ultimate strength state at the stress level of $0.56\sigma_Y$. Comparing this model with the model A + C, more distribution of yielding throughout the model members is observed, Fig. 11(c). The collapse characteristics of this model are more or less the same as those that were explained in the case of model A + C. Local tripping of stiffeners, local accumulation of plasticity in the plate and unloading throughout the model are experienced with almost more intensities in such a case, Fig. 11(d).

### 3.1.6. Summary

As is shown in Table 2 and Fig. 13, the present results are in good agreement with those of the other researchers [28]. The agreement is observed between the values of the buckling strength, ultimate strength and also the trends of the average stress–average strain relationships. The existing

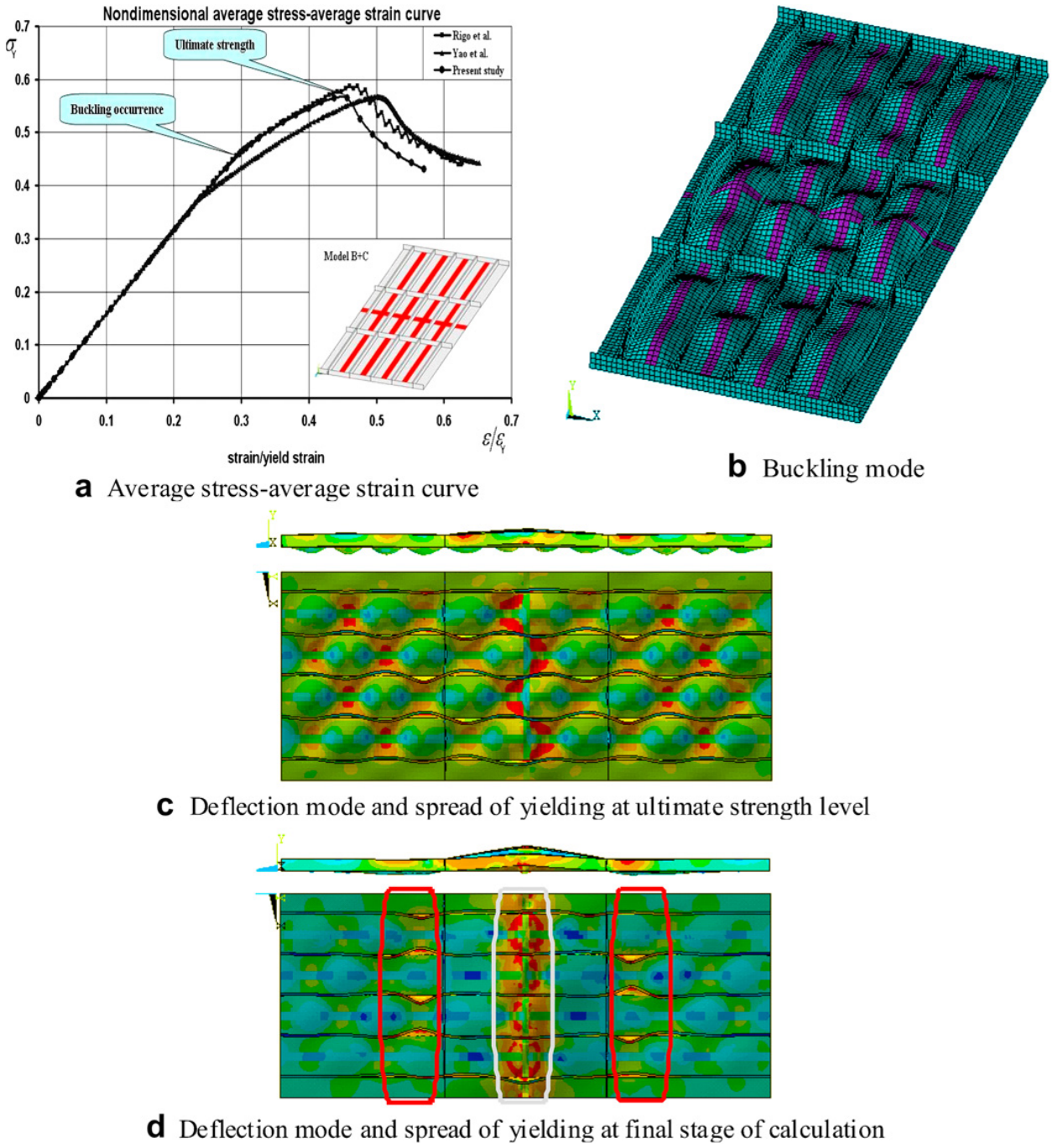


**Fig. 11.** Analysis results for model B + C under pure in-plane compression.

discrepancies among these load levels are mainly due to the differences in both modelling and discretisation methods adopted by different researchers [28].

Besides, it can be understood from Fig. 12 that the initial yielding stress for the case of model without HAZ is higher while that of the model B + C is least. The initial yielding stress for other models lies in between these two extreme values. The same behaviour is confirmed for the initial yielding strain of these models.

Model without HAZ exhibits the largest ultimate strength value, Fig. 14. This is due to the fact that no welding exists in the model and as a result no softening in the junctions as well as in the plate areas is created. The least value of the ultimate strength is obtained for the model A + C, Fig. 14. In such a model there is a combination of both longitudinal and transverse heat-affected zones. The longitudinal heat-affected zones exist along the junction lines of longitudinal stiffeners and plate, while the transverse heat-affected zone lies along the transverse centre line of the whole model.

**Table 2**
Comparison of the obtained results with those of the benchmark study of Rigo et al. [28].

| Contributors | Load-carrying | | Without HAZ (Reference) | With HAZ | | | |
|---|---|---|---|---|---|---|---|
| | | | | Model A | Model B | Model A + C | Model B + C |
| Rigo et al. [28] | Max. average stress(MPa) | Value | 173.46 | 150.22 | 171.21 | 129.12 | 151.61 |
| | | Difference to Reference(%) | Ref. | −13.40 | −1.30 | −25.56 | −12.60 |
| | Average strain (%) | | 0.321 | 0.300 | 0.324 | 0.232 | 0.269 |
| Lehmann et al. [28] | Max. average stress(MPa) | Value | 169.88 | 144.48 | 161.47 | 125.81 | 141.94 |
| | | Difference to Reference(%) | Ref. | −16.71 | −6.91 | −27.47 | −18.17 |
| | Average strain (%) | | 0.312 | 0.292 | 0.296 | 0.259 | 0.246 |
| Yao et al. [28] | Max. average stress (MPa) | Value | 160.80 | 136.15 | 157.7 | 126.1 | 146.28 |
| | | Difference to Reference (%) | Ref. | −15.33 | −1.93 | −21.58 | −9.03 |
| | Average strain (%) | | 0.321 | 0.310 | 0.322 | 0.265 | 0.285 |
| Present study | Max. average stress(MPa) | Value | 166.63 | 145.27 | 159.33 | 134.97 | 145.68 |
| | | Difference to Reference(%) | Ref. | −12.81 | −4.38 | −19.00 | −12.57 |
| | Average strain (%) | | 0.310 | 0.300 | 0.293 | 0.231 | 0.250 |

Application of extruded stiffeners as in case of model B (Fig. 14), leads to less reduction in the ultimate strength of the models in comparison with the reference case (model without HAZ). Model A shows a rapid decrease in the ultimate load carrying capacity of the structure under consideration. When adding transversal heat-affected zones to either model A or model B, resulting in models A + C and B + C, the ultimate strength as well as ultimate strain of the structure under consideration decreases significantly. Model B + C shows a much better strength characteristics than the model A + C, Fig. 14.

The buckling strength of the models does not exhibit any significant sensitivity versus the weld locations and combinations, Fig. 14.

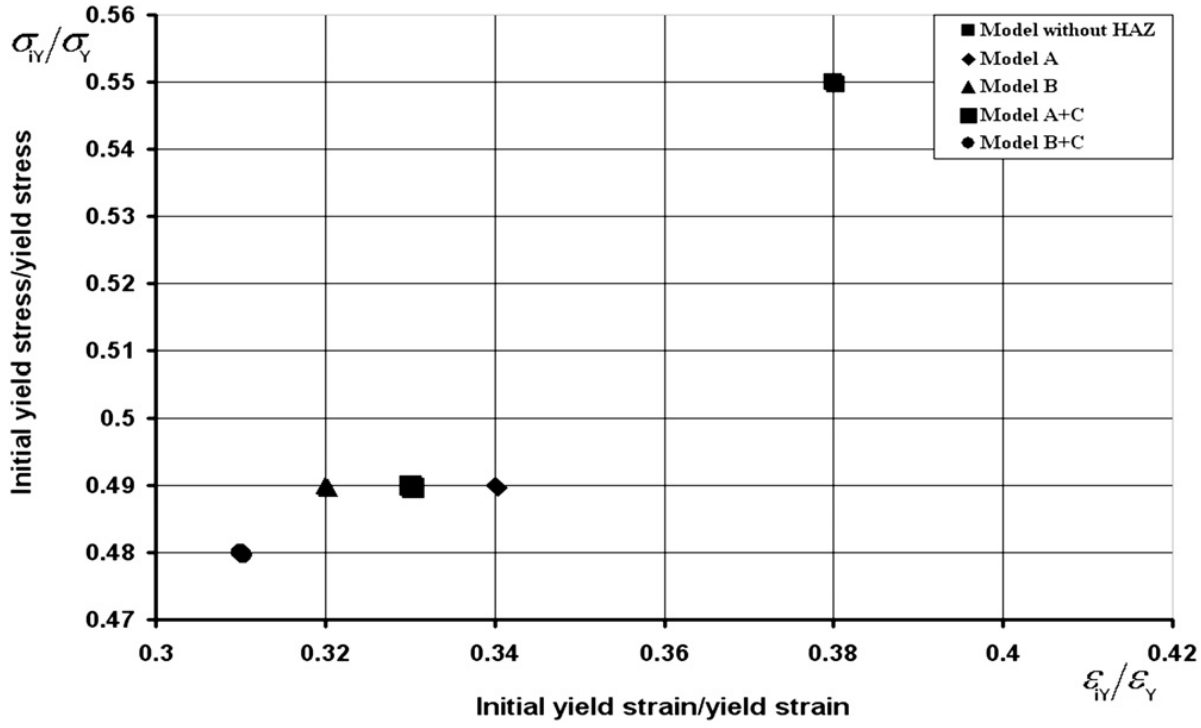


**Fig. 12.** Comparison of initial yielding stress values for the different models under pure in-plane compression based on the results of the present work.

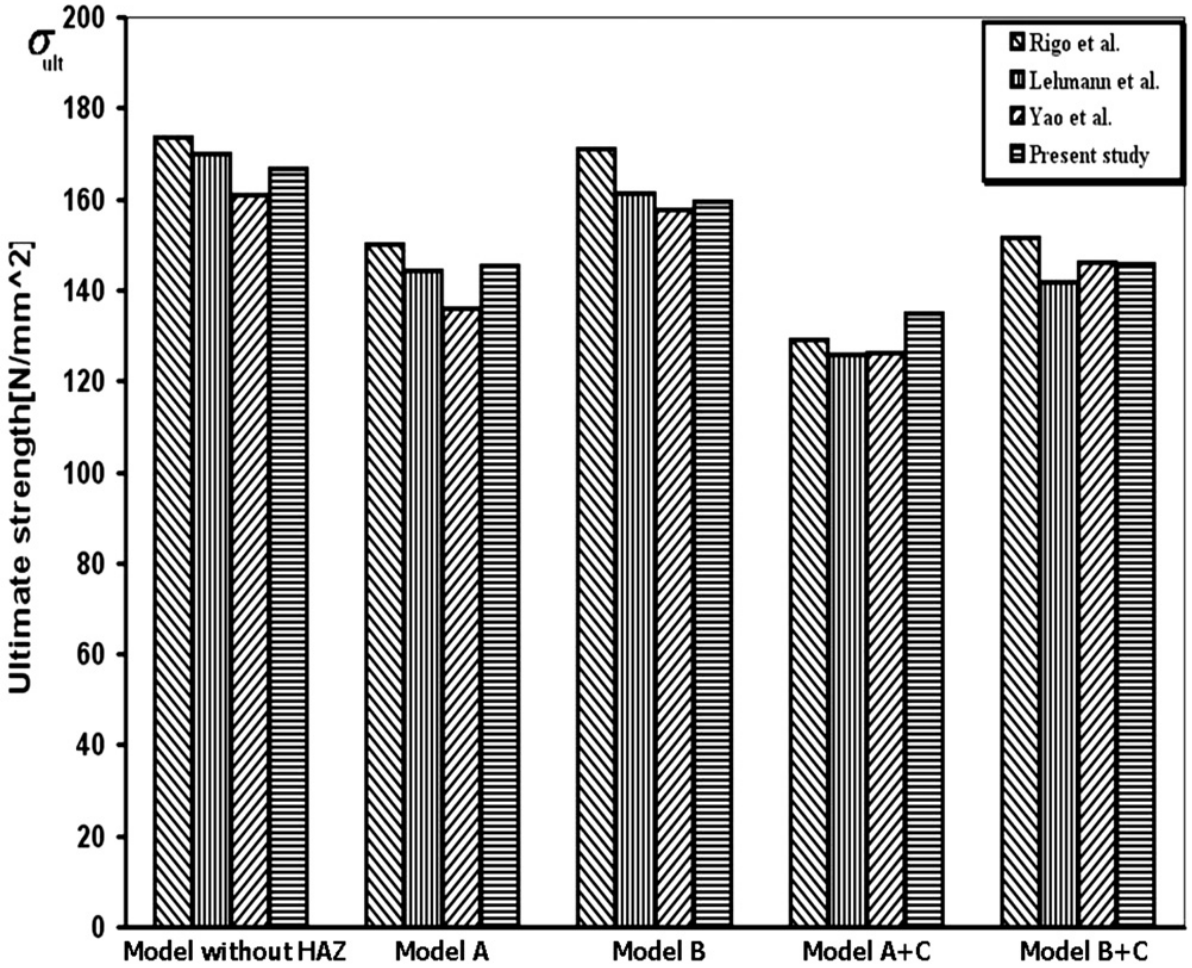


**Fig. 13.** Comparison of ultimate strength values for the models under pure in-plane compression based on the results of different researchers.

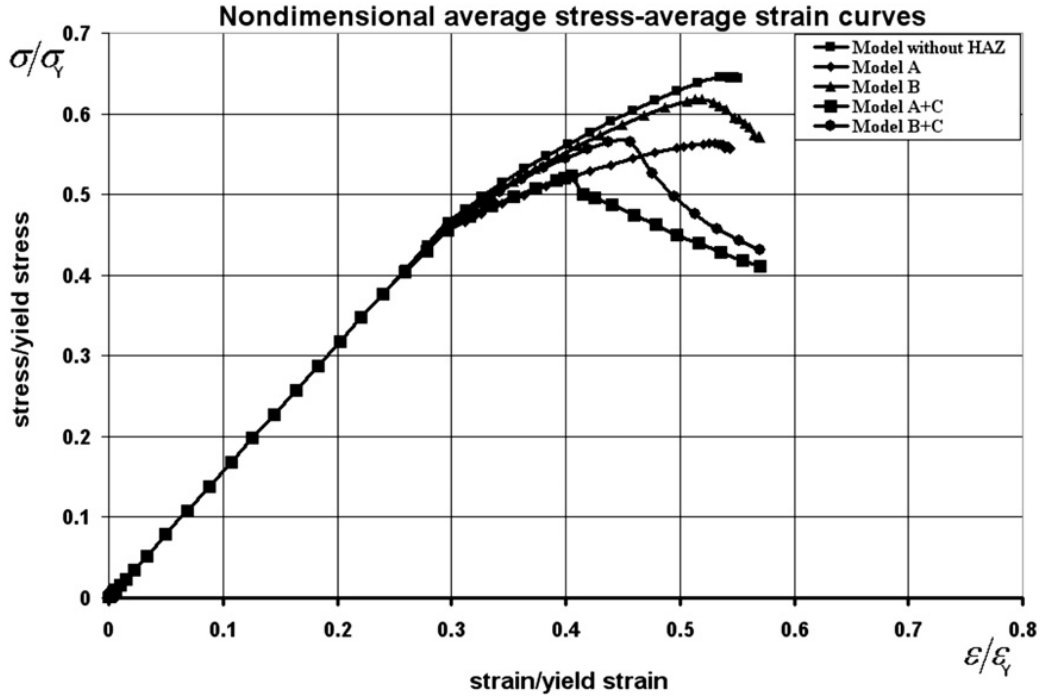


**Fig. 14.** Comparison of average stress–average strain relationships for the models under pure in-plane compression.

### 3.2. Post-buckling strength and behaviour under combined in-plane axial compression and lateral pressure

Figs. 15–19 show the average stress–average strain relationships of all models described before, under combined in-plane compression and lateral pressure. Also, the deflection modes and spreads of yielding for all models in such a loading condition are plotted in those figures. For a better understanding of sensitivity of the ultimate strength of all models when subjected to different magnitudes of lateral pressure in addition to the in-plane compression, Fig. 20 is prepared. Fig. 21 shows the ultimate compressive strength of all models under different levels of lateral pressure. In the following, the post-buckling behaviour and strength characteristics of these models under combined in-plane compression and lateral pressure are described in more details.

For a better understanding of what is discussed below, differences and similarities in the post-buckling behaviour of the analysed models under combined in-plane compression and lateral pressure are summarised in Table 3.

Generally, when the lateral pressure of 5–10 m is applied on the multi-stiffened aluminium plate, it is yielded just under the action of lateral load before application of any in-plane load. Based on the obtained results, it can be stated that the multi-stiffened aluminium plate deflects in a clamped mode under pure lateral load.

#### 3.2.1. Model without HAZ

Fig. 15(a) shows reduction in ultimate compressive strength as well as ultimate strain of model without HAZ when the magnitude of lateral pressure is increased. The trend of average stress–average strain curves also represents a regular decrease in the buckling strength and in-plane stiffness of the model when the lateral pressure increases.

When the model is subjected to a water head of up to 10 m, the model without HAZ reaches the state of ultimate strength in a simply-supported mode, Fig. 15(b). The larger the water head, the more irregular the buckling half-waves in both plate and stiffening members. The final collapse mode of the model under such magnitudes of lateral pressure has some different characteristics when compared with the case of pure in-plane compression. Unloading in the first and third spans together with concentration of plastic deformations in the middle span are outstanding features of the final collapse mode, Table 3.

Under a high lateral pressure of about 15 m, the model reaches the state of the ultimate load carrying capacity at a clamped mode, Fig. 15(b). The same mode is kept and followed until the final stage of collapse of the model. The longitudinal stiffeners almost experience collapse by accumulation of yielding in their ends as well as their mid-spans.

#### 3.2.2. Model A

The average stress–average strain relationships obtained for model A under combined in-plane compression and lateral pressure show a similar trend to those for the model without HAZ, Fig. 16(a). For such a model, when the lateral water head is up to 5 m (Fig. 16 (b)), the model reaches the ultimate strength state at a simply-supported mode. At the final stage of calculation under these values of water head, the plate panels and stiffening members have buckling mode of deflection, although the regularity of the half-waves are affected by the lateral pressure, Table 3.

With further increase of lateral pressure from 10 m above, the model reaches its ultimate strength state in a clamped mode, Fig. 16(b). The collapse mode of the model under such magnitudes of lateral pressure includes almost entire collapse of longitudinal stiffeners as well as accumulation of plastic deformations in the middle span of the model.

#### 3.2.3. Model B

Fig. 17(a) shows significant reduction in buckling strength, in-plane stiffness, ultimate strength and ultimate strain of model B when the magnitude of lateral pressure is increased in addition to the in-plane compressive load. As it can be observed from Fig. 17(b), apart from the case of pure in-plane compression, the simply-supported mode at the ultimate strength state and final collapse mode does not remain for much higher magnitudes of lateral pressure as was seen in the models without HAZ and A. For this model, the ultimate strength state as well as the final collapse takes place in the clamped

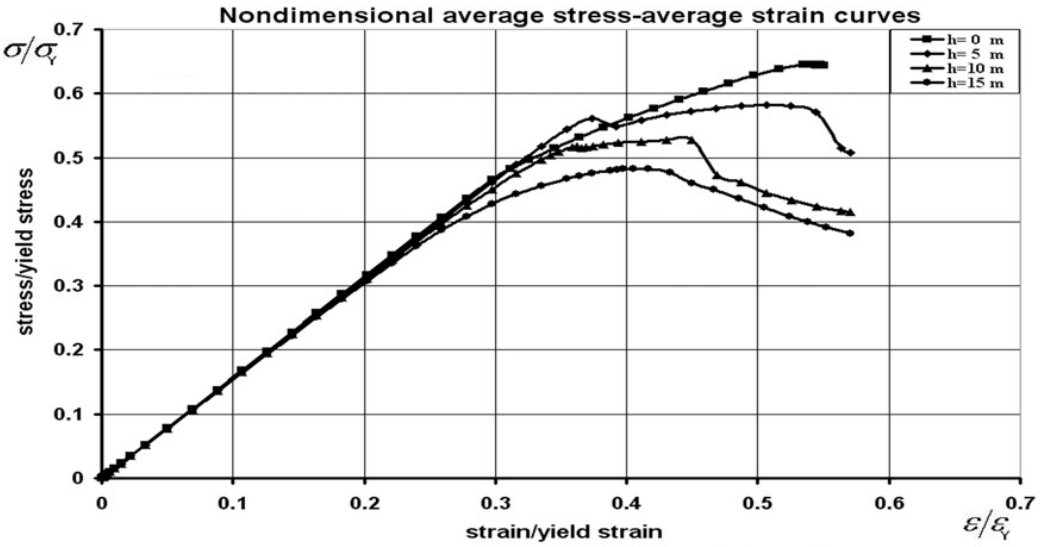


**a** Average stress-average strain relationship

**b** Deformation mode and Yielding extent

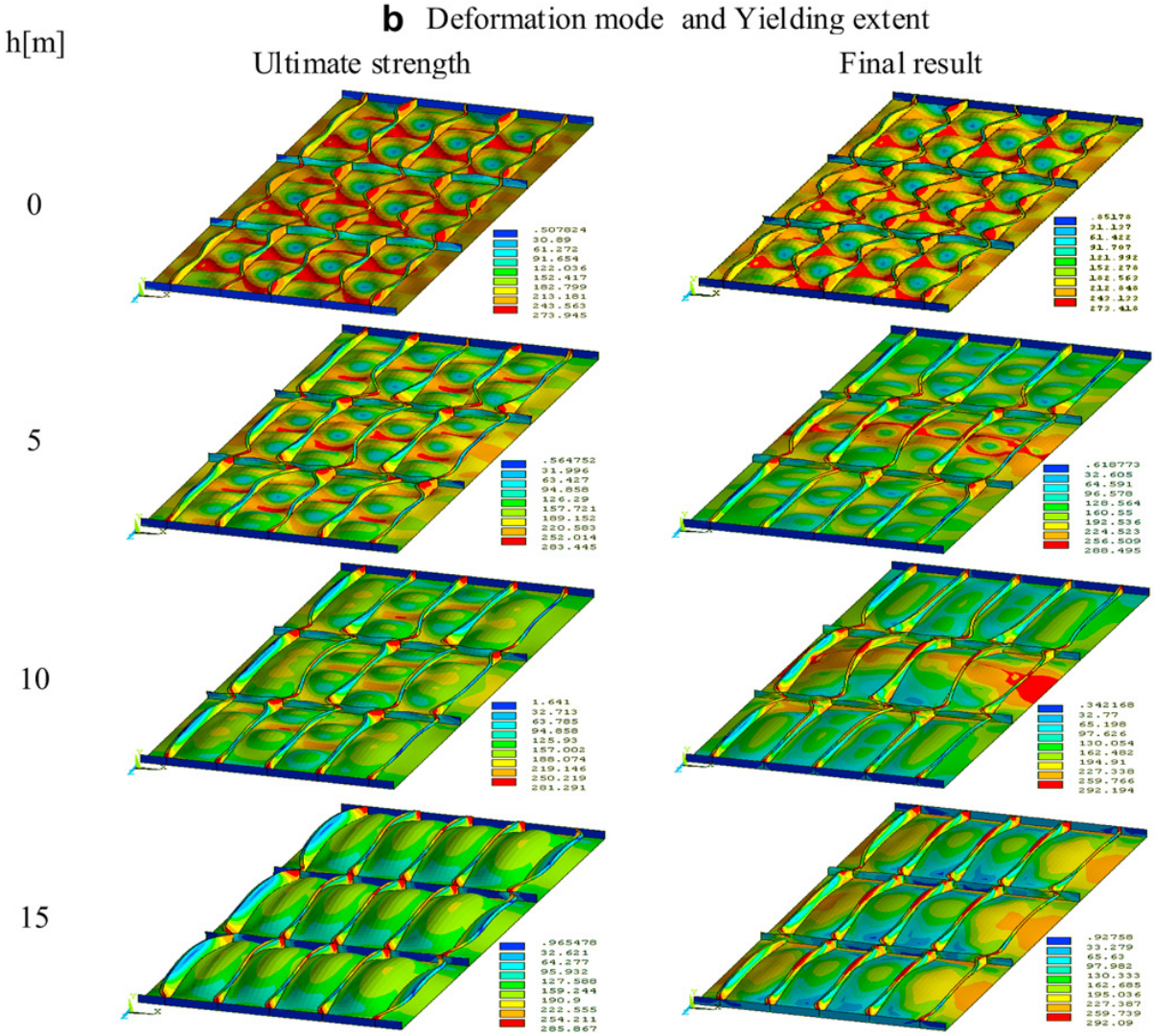


**Fig. 15.** Analysis results for model without HAZ under combined in-plane compression and lateral pressure.

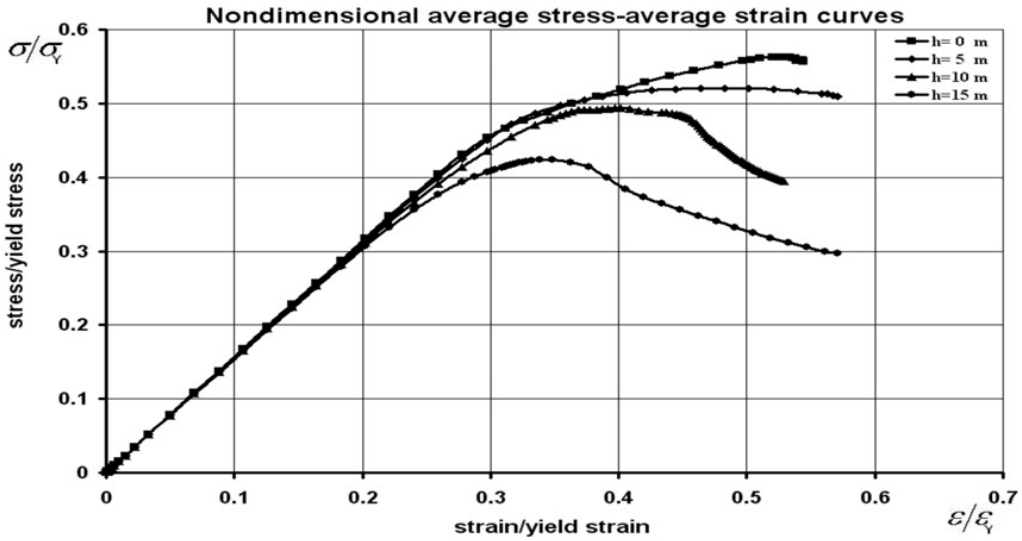


**a** Average stress-average strain relationship

**b** Deformation mode and Yielding extent

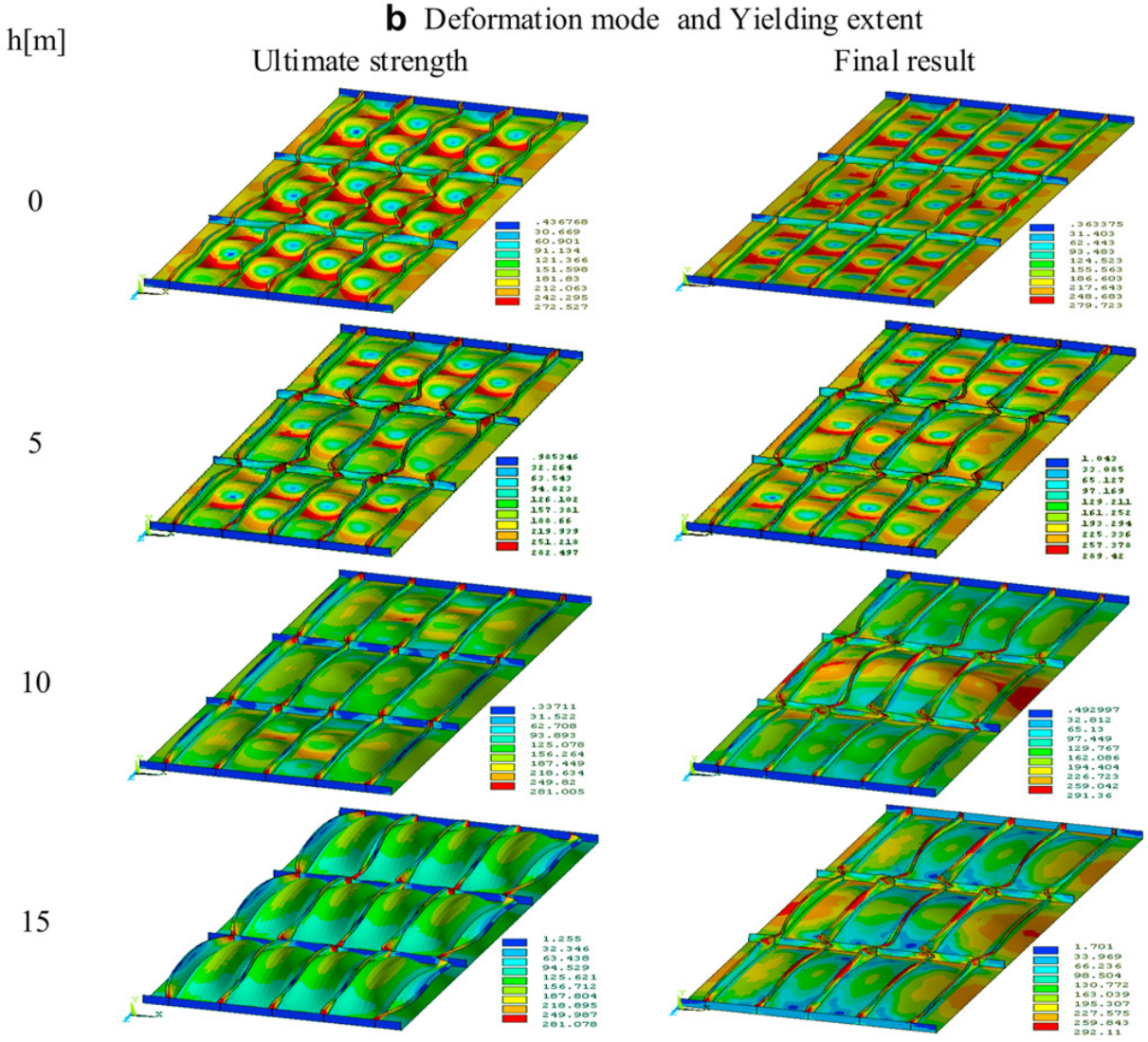


**Fig. 16.** Analysis results for model A under combined in-plane compression and lateral pressure.

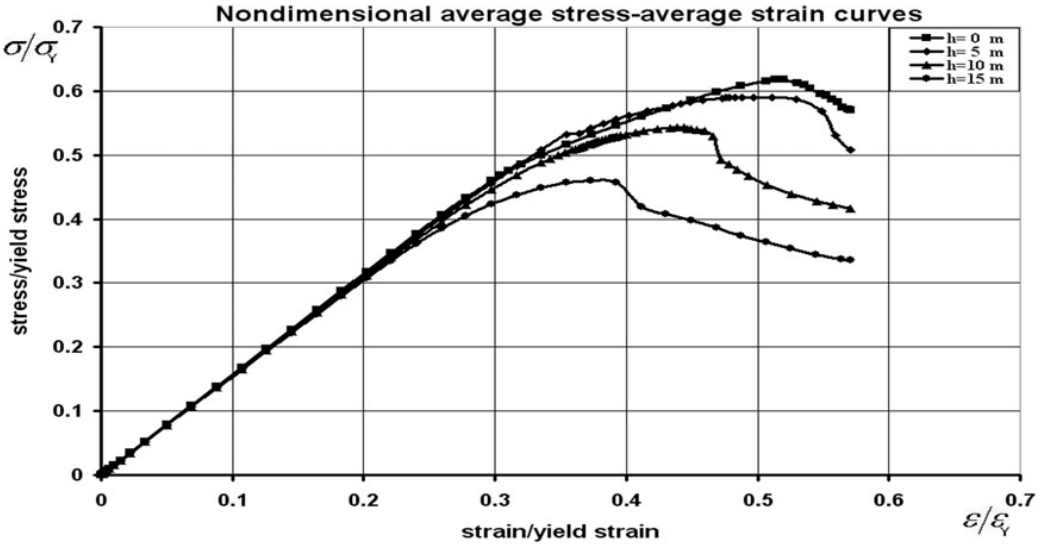


**a** Average stress-average strain relationship

**b** Deformation mode and Yielding extent

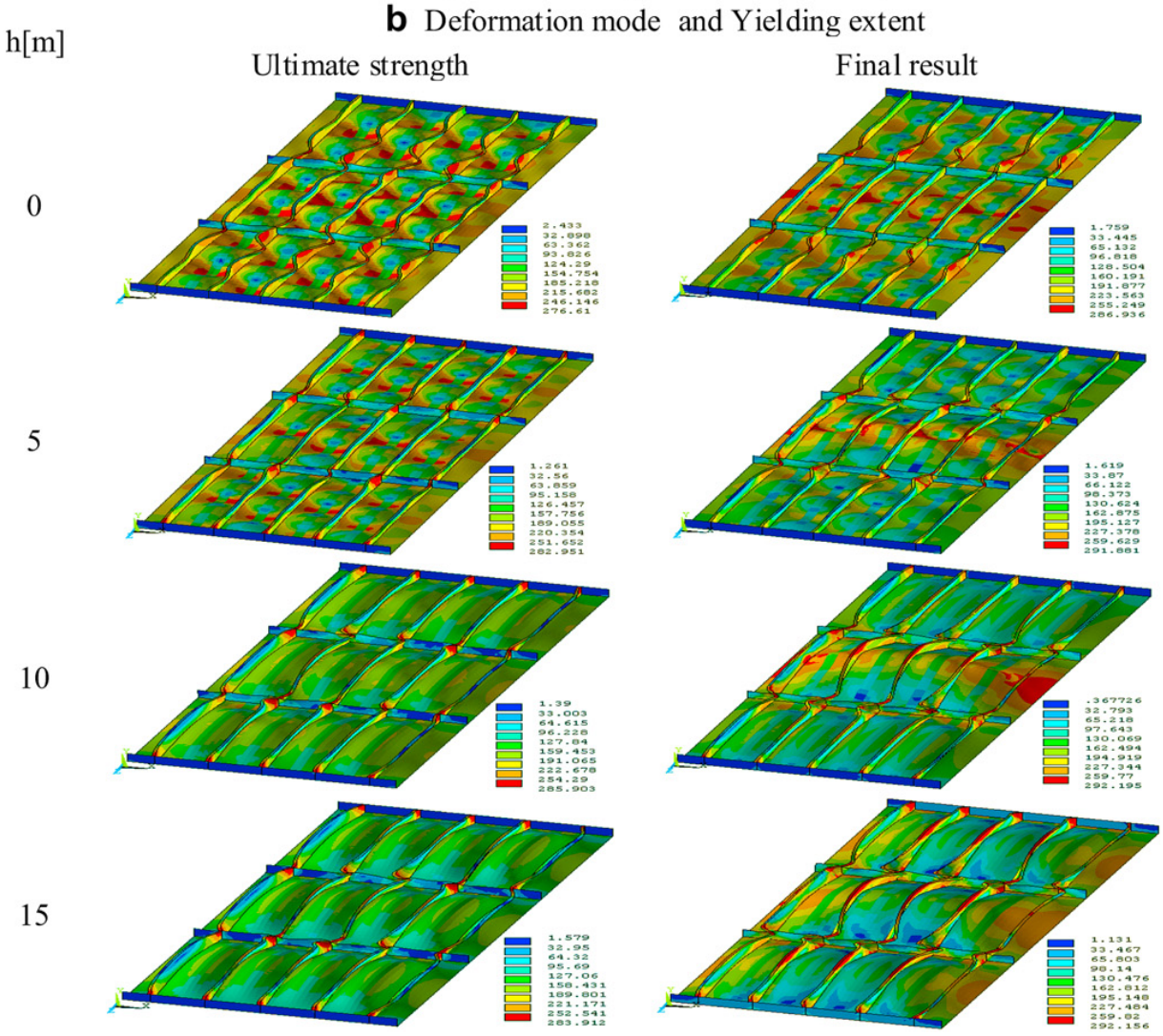


**Fig. 17.** Analysis results for model B under combined in-plane compression and lateral pressure.

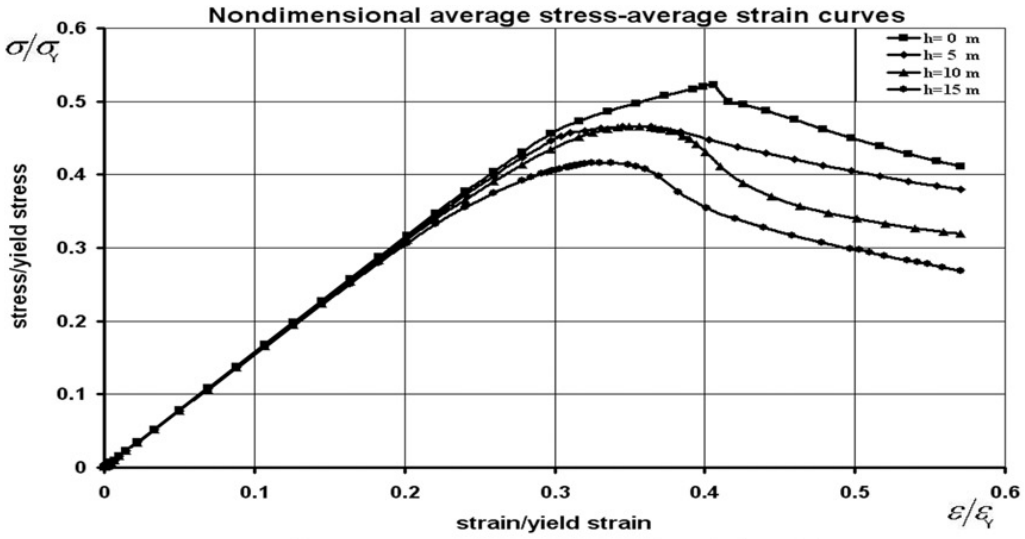


**a** Average stress-average strain relationship

**b** Deformation mode and Yielding extent

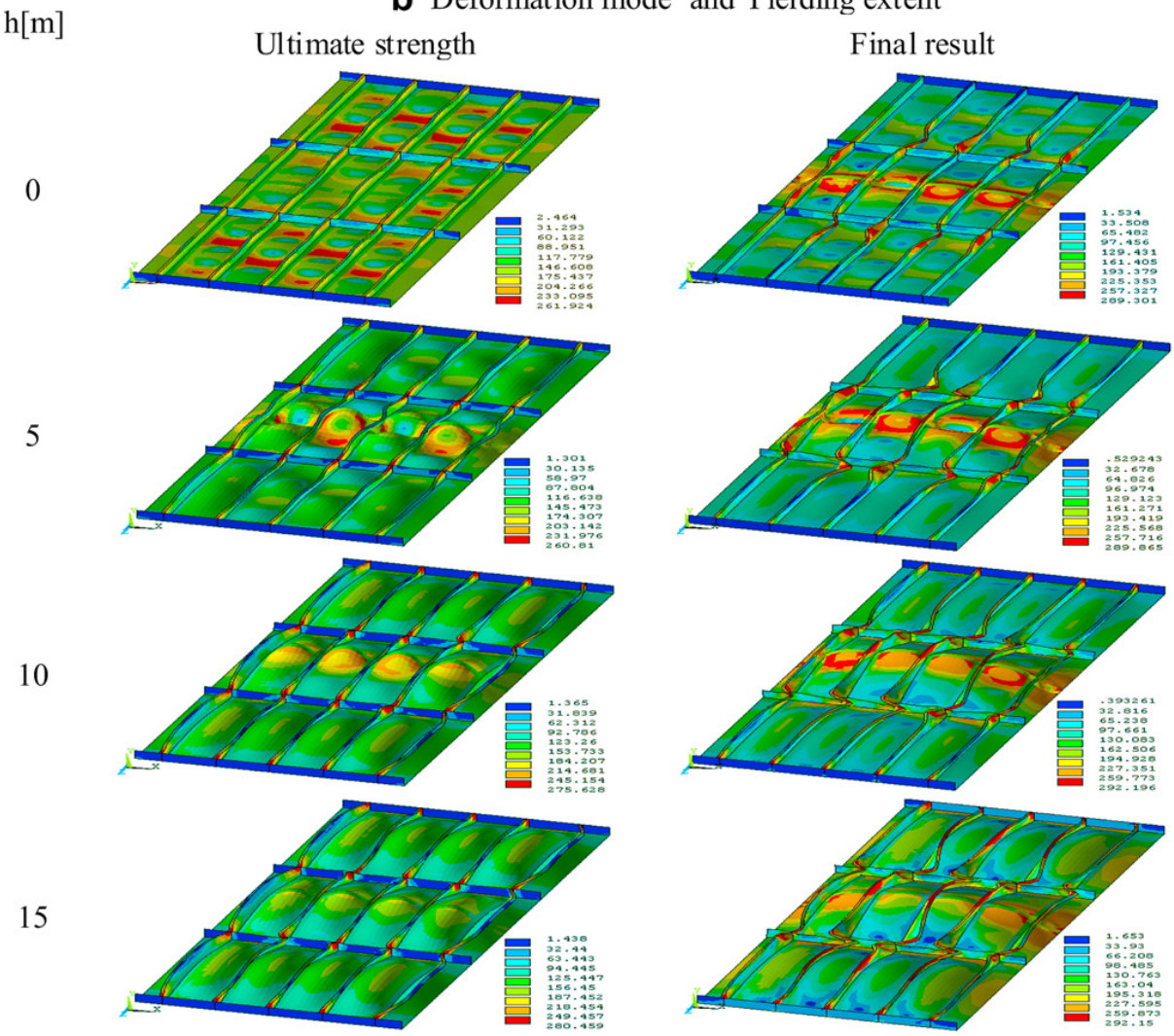


**Fig. 18.** Analysis results for model A + C under combined in-plane compression and lateral pressure.

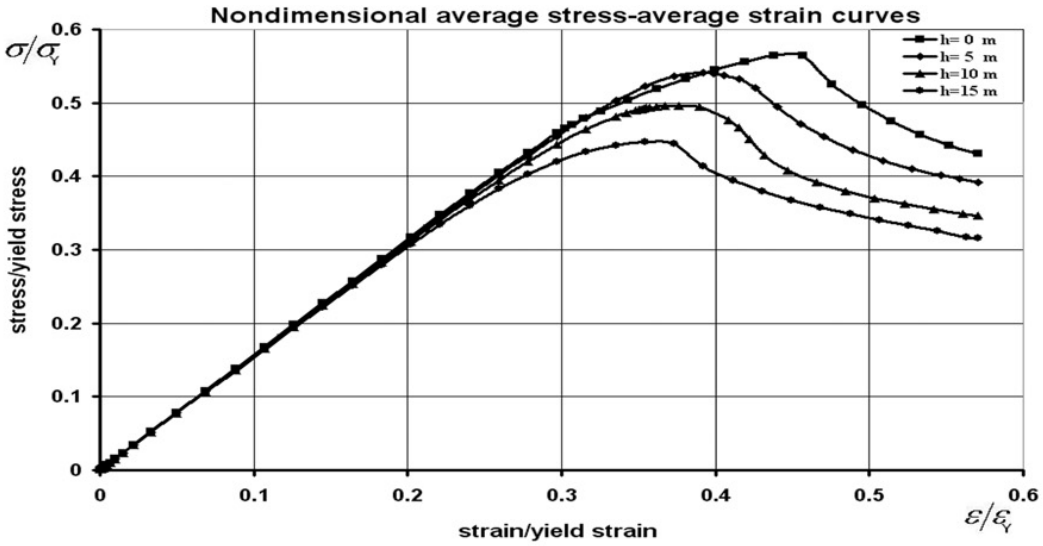


(a) Average stress-average strain relationship

(b) Deformation mode and Yielding extent

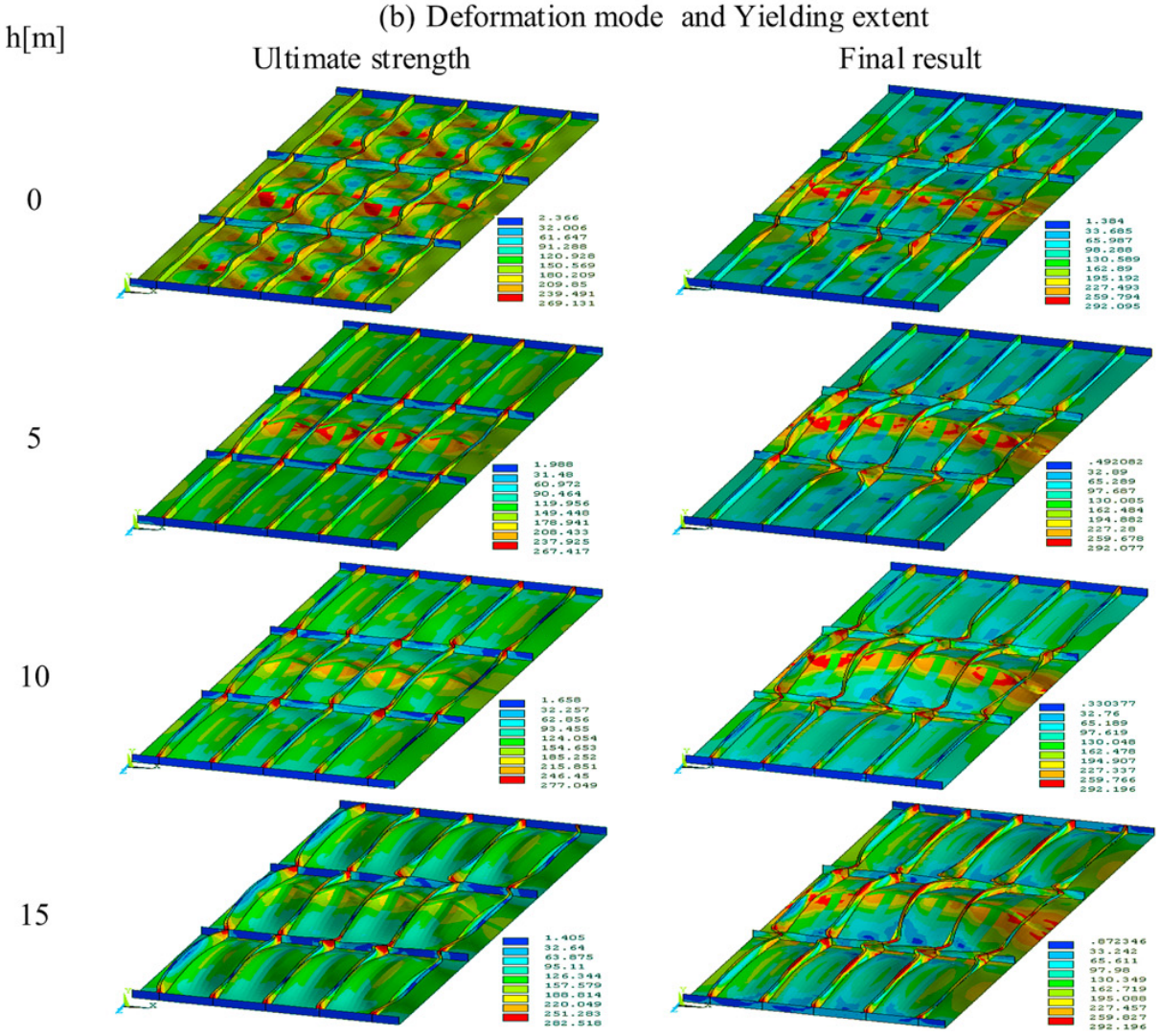


**Fig. 19.** Analysis results for model B + C under combined in-plane compression and lateral pressure.

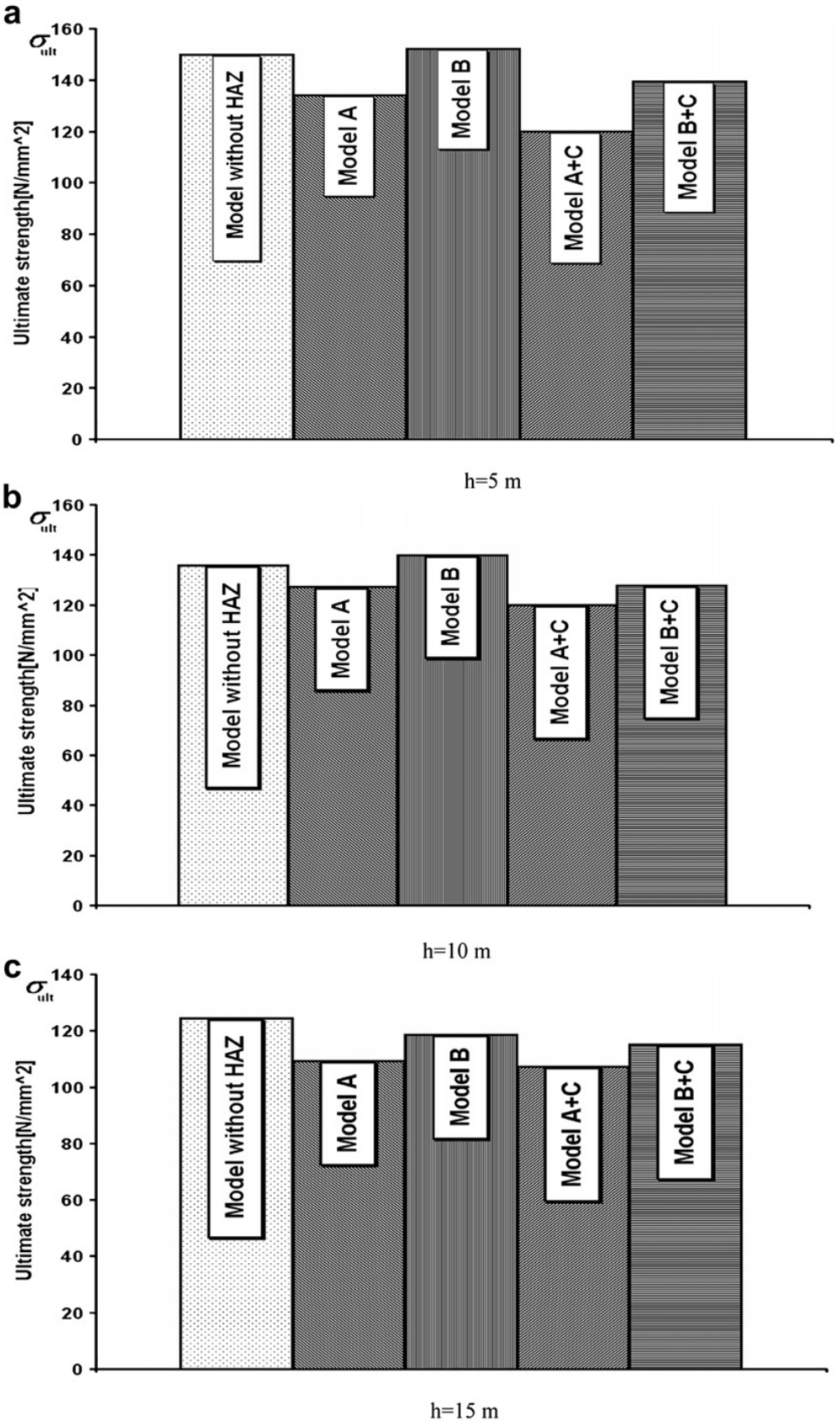


**Fig. 20.** Comparison of the obtained values of ultimate strength for different models under combined in-plane compression and lateral pressure.

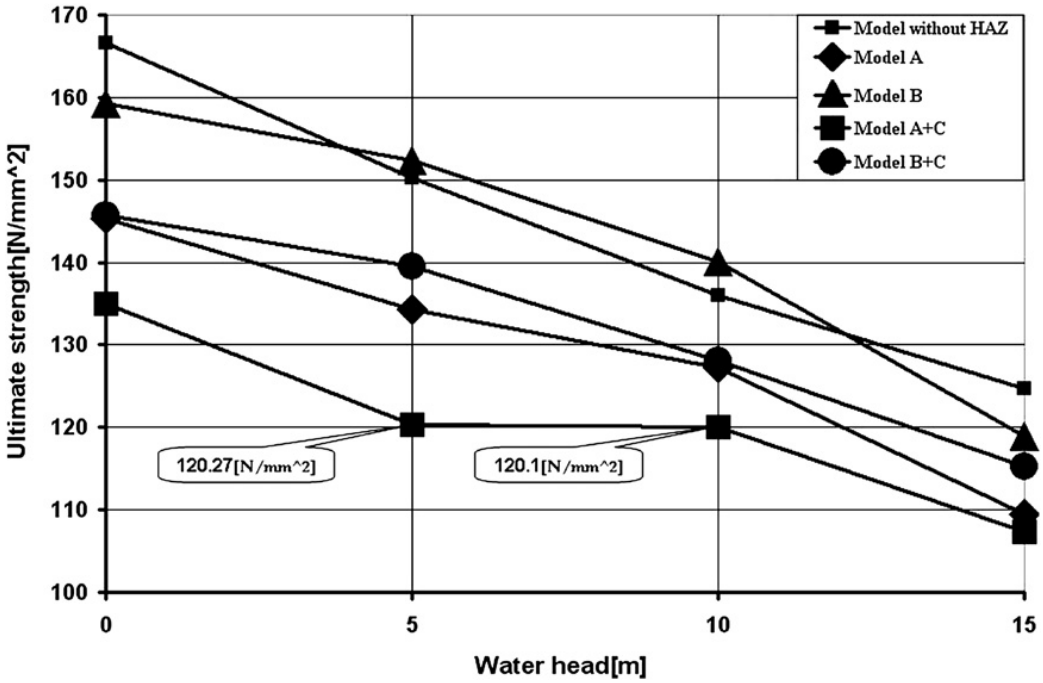


**Fig. 21.** Ultimate compressive strength for all models under different levels of lateral pressure.

mode for relatively high water heads. The clamped mode is in a form in which the stiffeners and attached plating deflects in an overall clamped way between the longitudinal weld lines. The final mode of collapse includes severe yielding of stiffener flanges and accumulation of local plastic deformations in the middle span of the whole model. The plate deforms in a bowing manner between longitudinal weld lines that connect the extruded stiffeners to each other. Deflection of plate enforces the stiffeners to rotate severely, Fig. 17(b) right column and Table 3.

### 3.2.4. Model A + C

The same strength and stiffness reduction characteristics as observed for model A are seen for the model A + C, Fig. 18(a). The ultimate strain-to-yield strain ratio of the model A falls in the interval of 0.33–0.55, while that of model A + C lies in the interval of 0.33–0.40, Figs. 16(a) and 18(a). For nonzero values of lateral pressure, the ultimate strength state of the model A + C is attained when the middle span of the model collapses (Fig. 18(b)). In all values of the lateral water head, final collapse of the model takes place in clamped mode for first and third spans and folded mode for the middle span, Fig. 18(b). The fold line of the model A + C in its middle span coincides exactly with the transverse weld line of the model. The twisting angle of stiffeners as well as yielding of their flanges is more magnified with the increase in the water head. Existence of the transversal weld line in model A + C does not change so much its ultimate compressive strength when compared with the model A, irrespective of the value of lateral pressure, Figs. 16 and 18(a), Table 3.

### 3.2.5. Model B + C

The same strength and stiffness reduction characteristics as observed for the model B are also experienced for model B + C, Fig. 19(a). The ultimate strain-to yield strain ratio of model B falls in the interval of 0.40–0.50, while that of model B + C lies in the interval of 0.35–0.45, Figs. 17 and 19(a). Post-ultimate strength regimes of the average stress–average strain curves for the model B + C show almost the same trends. Folding mode of deflection in the middle span of the model around the transversal weld line together with clamped mode of deflection in the other spans of the model are seen for lateral heads of around 10 above, Fig. 19(b). The clamped mode is in a form in which the stiffeners and attached plating deflects in an overall clamped way between the longitudinal weld lines. The stiffeners are more twisted in the higher water heads and yielding spreads in their flange regions.

**Table 3**
Differences and similarities in the post-buckling behaviour of the analysed models under combined in-plane compression and lateral pressure. (S.S.: Simply-Supported, C.: Clamped).

| Water Head [m] | Ultimate Strength | | | Final Collapse | | | |
|---|---|---|---|---|---|---|---|
| | Mode | Local Plate Buckling | Longitudinal Stiffener Buckling | Mode | Localised Plastic Deformation in Local Plate Panels | Localised Plastic Deformation in Longitudinal Stiffeners | Unloading |
| *Model without HAZ* | | | | | | | |
| 0 | S.S. | S.S. & Regular | S.S. & Regular | | Slight | Slight | Slight |
| 5 | S.S. | S.S. & Irregular | S.S. & Irregular | S.S. | Moderate in middle span-Slight in other spans | Moderate in middle span-Slight in other spans | Moderate in middle span-Slight in other spans |
| 10 | S.S. | S.S. & Irregular | S.S. & Irregular | C. | Moderate in middle span-Slight in other spans | Moderate in middle span-Slight in other spans | Moderate in middle span-Slight in other spans |
| 15 | C. | C. & Regular | C. & Regular | C. | Severe in all spans | Severe in all spans | Moderate in all spans |
| *Model A* | | | | | | | |
| 0 | S.S. | S.S. & Regular | S.S. & Regular | S.S. | Slight | Slight | Slight |
| 5 | S.S. | S.S. & Irregular | S.S. & Irregular | S.S. | Moderate in all spans | Moderate in all spans | Moderate in all spans |
| 10 | S.S. | S.S. & Irregular | S.S. & Irregular | C. | Severe in middle span-Slight in other spans | Severe in middle span-Slight in other spans | Moderate in all spans |
| 15 | C. | C. & Regular | C. & Regular | C. | Severe in all spans | Severe in all spans | Moderate in all spans |
| *Model B* | | | | | | | |
| 0 | S.S. | S.S. & Irregular | S.S. & Irregular | S.S. | Severe in middle span-Moderate in other spans | Moderate in middle span-Severe in other spans | Slight in middle span-Moderate in other spans |
| 5 | C. | C. & Regular | C. & Regular | C. | Severe in middle span-Moderate in other spans | Severe in middle span-Moderate in other spans | Slight in middle span-Moderate in other spans |
| 10 | C. | C. & Regular | C. & Regular | C. | Severe in middle span-Moderate in other spans | Severe in middle span-Moderate in other spans | Slight in middle span-Moderate in other spans |
| 15 | C. | C. & Regular | C. & Regular | C. | Severe in all spans | Severe in all spans | Moderate in all spans |

(*continued on next page*)

**Table 3** (*continued*)

| Water Head [m] | Ultimate Strength | | | Final Collapse | | | |
|---|---|---|---|---|---|---|---|
| | Mode | Local Plate Buckling | Longitudinal Stiffener Buckling | Mode | Localised Plastic Deformation in Local Plate Panels | Localised Plastic Deformation in Longitudinal Stiffeners | Unloading |
| *Model A + C* | | | | | | | |
| 0 | S.S. | S.S. & Irregular | S.S. & Irregular | S.S.+Folding in middle span | Severe in middle span-Moderate in other spans | Moderate in middle span-Severe in other spans | Moderate in all spans |
| 5 | S.S.+Folding in middle span | S.S. & Irregular | S.S. & Irregular | S.S.+Folding in middle span | Severe in middle span-Moderate in other spans | Severe in middle span-Moderate in other spans | Moderate in all spans |
| 10 | C.+Folding in middle span | S.S. & Irregular | S.S. & Irregular | C.+Folding in middle span | Severe in middle span-Moderate in other spans | Severe in middle span-Moderate in other spans | Moderate in all spans |
| 15 | C.+Folding in middle span | C. & Regular | C. & Regular | C.+Folding in middle span | Severe in all spans | Severe in all spans | Slight in all spans |
| *Model B + C* | | | | | | | |
| 0 | S.S.+Folding in middle span | S.S. & Irregular | S.S. & Irregular | S.S.+Folding in middle span | Severe in middle span-Moderate in other spans | Moderate in middle span-Severe in other spans | Moderate in all spans |
| 5 | S.S.+Folding in middle span | S.S. & Irregular | S.S. & Irregular | S.S.+Folding in middle span | Severe in middle span-Moderate in other spans | Severe in middle span-Moderate in other spans | Moderate in all spans |
| 10 | C.+Folding in middle span | S.S. & Irregular | S.S. & Irregular | C.+Folding in middle span | Severe in middle span-Moderate in other spans | Severe in middle span-Moderate in other spans | Moderate in all spans |
| 15 | C.+Folding in middle span | C. & Regular | C. & Regular | C.+Folding in middle span | Severe in all spans | Severe in all spans | Slight in all spans |

The ultimate strength of model B + C for any value of lateral pressure slightly drops down that of model B for the same value of lateral pressure, Figs. 17 and 19(a), Table 3.

*3.2.6. Summary*

Figs. 20 and 21 show that neglecting the exceptional cases, the model without HAZ and model A + C exhibit maximum and minimum values of the ultimate strength, respectively, for any value of water head. The strength of model B, model B + C and model A fall between the strength of the other two extreme models, for any value of water head.

Model B is constructed from extruded stiffeners. The weld lines between extruded stiffeners lie longitudinally in the middle of plate panels. When lateral pressure is about 5–10 m, the plate panels and attached stiffeners in model B tend to deflect in a clamped mode, Fig. 17(b). This is while in case of model without HAZ, still the plate and its stiffening members deflect in a simply-supported mode under such values of lateral pressure. That is why the ultimate strength of model B becomes higher than that of model without HAZ for water heads of 5–10 m, Fig. 21. For water head of 15 m, both models deflect in a clamped mode, but overall bending of stiffened plate panels between the longitudinal weld lines in a clamped mode in addition to the clamped mode deflection of local plate panels lead to more reduction of the ultimate capacity of the model B in comparison with that of model without HAZ under 15 m water head.

## 4. Conclusions

A numerical investigation was made to study the effect of lateral pressure on the post-buckling behaviour and strength characteristics of stiffened aluminium plates subjected to in-plane compression. Different models incorporating various welding arrangements as well as stiffeners were analysed. The main conclusions in brief are:

- Under pure in-plane compression
- Existence and arrangement of weld lines does not have significant effect on the initial buckling strength of the models.
- Post-buckling behaviour and strength characteristics of the models are much influenced by both the type of stiffeners (extruded or welded up) and welding arrangements.
- Transverse weld lines in connection with longitudinal ones changes the collapse mode of the stiffened aluminium models to a mode in which tripping mechanisms in stiffeners as well as local accumulation of plastic deformations in plate are experienced.
- Under combined in-plane compression and lateral pressure
- Existence and arrangement of weld lines does not have significant effect on the trends of the average stress–average strain relationships of any specific model under different values of lateral pressure.
- Post-buckling behaviour and strength characteristics of the models are highly dependent on the magnitude of lateral pressure, existence and arrangement of weld lines.
- Transverse weld lines lead to the creating folding pattern of deflection in central span of the models while yielding spreads in the stiffeners.
- Under small magnitudes of lateral pressure, the local plate panels and their supporting members deflect in simply-supported mode. Besides, folding patterns are also created in some cases.
- With increase in the magnitude of lateral pressure, the deflection mode of both plate panels and stiffening members tend to be in a clamped mode. Again folding modes are observed in some cases especially in the middle span.
- The model A + C exhibits minimum value of the ultimate strength, for any value of water head.
- The model without HAZ or model B represents maximum ultimate strength depending on the level of lateral load.

It is believed that the explored post-buckling behaviours and strength characteristics would be very much useful for simulation of average stress–average strain relationships of multi-stiffened aluminium

plates subject to combined in-plane compression and lateral pressure when assessment of ultimate strength of aluminium ships.

## References


[1] Murray NW. Buckling of stiffened panels loaded axially and in bending. Structure Engineering 1973;51(8):285–301.
[2] Dorman AP, Dwight JB. Tests on stiffened compression panels and plate panels. In: Proceedings of the international conference on steel box girder bridges. London: The Institution of Civil Engineers; February 1973. p. 63–75.
[3] Smith CS. Compressive strength of welded steel ship grillages. Transactions of the Royal Institution of Naval Architects 1975;117:325–47.
[4] Horne MR, Narayanan R. Ultimate strength of stiffened panels under uniaxial compression. In: Dowling PJ, Harding JE, Frieze PA, editors. Proceedings of the International Conference on Steel Plated Structures, Imperial College, London, July 1976. Crosby Lockwood Staples; 1977. p. 1–23.
[5] Dowling PJ, Moolani FM, Frieze PA. The effect of shear lag on the ultimate strength of box girders. In: Dowling PJ, Harding JE, Frieze PA, editors. Proceedings of The International Conference on Steel Plated Structures, Imperial college, London, July 1976. Crosby Lockwood Staples; 1977. p. 108–41.
[6] Faulkner D. Compression tests on welded eccentrically stiffened plate panels. In: Dowling PJ, Harding JE, Frieze PA, editors. Proceedings of the international conference on steel plated structures, Imperial college, London, July 1976. Crosby Lockwood Staples; 1977. p. 581–617.
[7] Tanaka Y, Endo H. Ultimate strength of stiffened plates with their stiffeners locally buckled in compression. Journal of the Society of Naval Architects of Japan 1988:164 [in Japanese].
[8] Dow RS. Testing and analysis of a 1/3-scale welded steel frigate model. In: Smith CS, Dow RS, editors. Advances in marine structures—2. Elsevier; 1991.
[9] Ghavami K. Experimental study of stiffened plates in compression up to collapse. Journal of Constructional Steel Research 1994;28(2):197–222 [Special Brazilian Issue, Guest Editor Khosrow Ghavami].
[10] Grondin GY, Chen Q, Elwi AE, Cheng JJ. Stiffened steel plates under compression and bending. Journal of Constructional Steel Research 1998;45(2):125–48.
[11] Miller M, Nadeau J, White GJ. Longitudinally stiffened panels – a comparative analysis of the compressive strength of three common construction methods. Proceedings of SNAME annual meeting; 1999.
[12] Sherbourne AN, Liaw CY, Marsh C. Stiffened plates in uniaxial compression. IABSE 1971;31:145.
[13] Carlsen CA. Simplified collapse analysis of stiffened plates. Norwegian Maritime Research 1977;4:20–36.
[14] Moolani FM, Dowling PJ. Ultimate load behaviour of stiffened plates in compression. Steel plates structures. In: Dowling PJ, Harding JE, Frieze PA, editors. Proceedings of the International Conference on Steel Plated Structures, Imperial College. London: Crosby Lockwood Staples; July 1976. p. 51–88.
[15] Guedes Soares C, Soreide TH. Behaviour and design of stiffened plates under predominantly compressive loads. International Shipbuilding Progress 1983:341.
[16] Chapman JC, Smith CS, Davidson PC, Dowling PJ. Recent developments in the design of stiffened plate structures. Transactions of the Royal Institution of Naval Architects 1989.
[17] Bonello MA, Chryssanthopoulos MK, Dowling PJ. Ultimate strength design of stiffened plates under axial compression and bending. Marine Structures 1993;6:533–52.
[18] Chen Q, Zimmerman TJE, DeGeer D, Kennedy BW. Strength and stability testing of stiffened plate components. Ship structural committee report SSC-399; 1997.
[19] Grondin GY, Elwi AE, Cheng JJR. Buckling of stiffened plates- a parametric study. Journal of Constructional Steel Research 1999;50:151–75.
[20] Clarke JD, Narayanan R. Buckling of aluminium alloy stiffened plate ship structure. In: Proceedings of the International Conference on Steel and Aluminium Structures, Cardiff, July 1987; Aluminium structures—advances design and construction. Elsevier; 1987. p. 81–92.
[21] Aalberg A, Langseth M, Larsen PK. Stiffened aluminium panels subjected to axial compression. Thin Walled Structure 2001;39:861–85.
[22] Aalberg A, Langseth M, Malo KA. Ultimate strength of stiffened aluminium plates. Norwegian University of Science and Technology, Department of Structural Engineering; 1998.
[23] Kristensen QHH, Moan T. Ultimate strength of aluminium plates under biaxial loading. In: Proceedings of the fifth international conference on fast sea transportation. New York; 1999.
[24] Zha Y, Moan T, Hanken E. Experimental and numerical study of torsional buckling of stiffeners in aluminium panels. In: Proceedings of the fifth International Conference on ISOPE. Seattle; May 2000. p. 249–55.
[25] Zha Y, Moan T, Hanken E. Ultimate strength of stiffened aluminium panels with predominantly torsional failure modes. Thin Walled Structure 2001;39:631–48.
[26] Zha Y, Moan T. Experimental and numerical prediction of collapse of flatbar stiffeners in aluminium panels. Journal of Structural Engineering 2003;129(2):160–8.
[27] Hopperstad OS, Langseth M, Hanssen L. Ultimate compressive strength of plate elements in aluminium: correlation of finite element analyses and tests. Thin Walled Structure 1998;29:31–46.
[28] Rigo P, et al. Sensitivity analysis on ultimate strength of aluminium stiffened panels. Marine Structures 2003;16:437–68.
[29] Paik JK, Duran A. Ultimate strength of aluminium plates and stiffened panels for marine applications. Journal of Marine Technology 2004;41(3):108–21.
[30] ANSYS user's manual (Version 7.1). Houston: Swanson Analysis Systems Inc; 2003.
[31] Cook RD, Malkus DS, Plesha ME, Witt RJ. Concepts and applications of finite element analysis. 4th ed. John Wiley & Sons, Inc; 2002.
[32] Paik JK, Thayamballi AK. Ultimate limit state design of steel plated structures. 1st ed. John Wiley & Sons, Inc; 2003.